Sulphate concentration in cave dripwater and speleothems: long-term trends and overview of its significance as proxy of environmental processes and climate changes

Andrea Borsato[1*], Silvia Frisia[1], Peter Wynn[2], Ian J. Fairchild[3], Renza Miorandi[4]

[1] *School of Environmental and Life Sciences, The University of Newcastle, Callaghan, NSW 2308, Australia*

[2] *Lancaster Environment Centre, University of Lancaster, Lancaster,LA1 4YQ, UK.*

[3]*School of Geography, Earth and Environmental Sciences, University of Birmingham, Birmingham, Edgbaston, B15 2TT, UK*

[4]*Gruppo Grotte S.A.T. "Emilio Roner", 38068 Rovereto (TN), Italy.*

* Corresponding author: *andrea.borsato@newcastle.edu.au*

Keywords: Sulphur, speleothems; karst water; volcanic eruptions; anthropogenic sulphur peak.

Abstract

Sulphate concentration in speleothems identifies major volcanic eruptions, provide useful information on soil and aquifer dynamics and, similarity to the ^{14}C bomb peak, its Anthropocene peak can be used to date recent cave formations. However, the transmission of S from the atmosphere to cave dripwater and its incorporation in speleothems is subjected to biogeochemical cycling and accurate studies of

each cave site are needed in order to assess how the S atmospheric signal is modified and eventually encoded in speleothems.

This study investigates the role of biogeochemical cycling and aquifer hydrology by utilising published and new dripwater and speleothem data from Grotta di Ernesto (ER) in northern Italy. Here we provide the first long-term record of sulphate concentration in cave dripwater based on over 20 years of measurements. Fast drip site st-ER1 is characterised by a continuous decrease in SO_4 concentration from a high of 7.5 ±0.8 mg/l in 1993-1994 to a low of 2.2 ±0.2 mg/l in 2013-2014, and replicates with a delay of ~15 years the decline in the atmospheric SO_2 emissions. The S-series of slow flow ER78 site is further delayed by ~4.5 years in relation to the S retention in the aquifer matrix. The dripwater data are used to extend the previously published S record (1810 – 1998 AD) of stalagmite ER78 and reconstruct the anthropogenic S-peak: this displays a delay of ~20 years with respect to the atmospheric S emission peak due to biogeochemical cycling and aquifer storage. However, sulphur recycling above the cave did not operate with the same degree of efficiency through time, which resulted in a variable time delay between S deposition and incorporation into the stalagmite. In the pre- Anthropocene era, and in particular during the cold Little Ice Age, biogeochemical cycling was far less efficient than today, and the fast transmission of the atmospheric signal allowed capture of S released during major volcanic eruptions by stalagmites.

1. Introduction

Sulphur concentration in Greenland ice cores provided the first evidence of the impact of anthropogenic SO_2 emissions on regional climate following industrialisation in the Northern Hemisphere (Neftel et al., 1985; Mayewski et al., 1986). The detailed chemical investigation of

Greenland and Alpine ice cores provided further insight into the influence of natural and anthropogenic sulphur sources on atmospheric SO_4 load and led to the identification of volcanic eruptions characterised by high explosivity (Wagenbach et al., 1988; Legrand and Mayewski, 1997; Schwikowski et al., 1999; Preunkert et al., 2001; Bigler et al., 2002; Patris et al., 2002). The record of a high-elevation (4450 m asl) ice cap in the Monte Rosa massif indicated that natural SO_4 sources as sea-spray, mineral dust and quiescent volcanic emissions accounted for the S atmospheric signal during pre-industrial periods, but that their combined contribution diminished progressively below 10-15% in the course of the 20th century as a consequence of the increasing anthropogenic emissions (Schwikowski et al., 1999). During pre-industrial time, major volcanic eruptions significantly increased the dust and aerosol concentration (including SO_4) in the atmosphere, causing climate perturbation lasting several years. However, the lack of ice core archives at mid-latitudes and at low elevations limits our understanding of the role of both natural and anthropogenic aerosols in modifying regional climate. In these settings, carbonate speleothems (stalagmites and stalactites) provide complementary information by capturing changes in the atmospheric composition as well as climate signals through a range of isotopic and elemental proxies (McDermott, 2004; Fairchild and Treble, 2009).

Stalagmites are known to record atmospheric sulphur loads and ecosystem dynamics in karst regions, thus expanding the inventory of trace element proxies extracted from speleothems to a level commensurate with ice cores (Frisia et al., 2005, 2008; Wynn et al., 2008, 2010, 2013). Sulphur concentration trends in stalagmites were related to anthropogenic emissions starting in the late 19th century (Frisia et al., 2005, 2008; Uchida et al., 2013). It was also suggested that discrete S peaks in stalagmites record high explosivity index volcanic eruptions (Frisia et al., 2005, 2008; Badertscher et al., 2014). Contrary to ice cores, the transmission of S from the atmospheric deposition to cave dripwater and its incorporation in speleothems is not direct. It can be subjected to biogeochemical cycling in the soil and vegetation above the cave, which is highly efficient in forested catchments (eg.

Likens et al., 2002; Shanley et al., 2005; Novak et al., 2007). These processes potentially modify the S concentration and S isotopic signature in stalagmites, as well as delay the transmission of the sulphur atmospheric signal into the epikarst (Wynn et al., 2013).

In a review of the literature on sulphur cycling in forested catchments, Wynn et al. (2013) highlighted that biogeochemical cycling may retain sulphur in the soil and vegetation overlying the cave system through processes of inorganic adsorption as well as biologically mediated processes of: i) assimilation, which is the uptake and incorporation of sulphate into soil microorganisms and vegetation; ii) mineralisation, which is the conversion of carbon bonded sulphur compounds released from decaying vegetation and soil organic matter into sulphate; iii) oxidation, which is the incorporation of oxygen into inorganic sulphides; and iv) dissimilatory reduction, which is the removal of oxygen from sulphur compounds to ultimately produce H_2S, occurring under reducing conditions. Fast infiltration events and/or infiltration where soil is thin and vegetation cover is scarce allow quick flow through the soil zone. In this case, preferential flow routing through epikarst results in speleothem capture of a sulphate signal largely unmodified with respect to the atmospheric source. Most commonly, the biogeochemical cycling of sulphur through vegetation and soils and the successive mixing with stored soil and aquifer sources will delay, concentrate and fractionate the S chemical or isotopic signal in dripwater and, eventually, speleothems (Wynn et al., 2008, 2010, 2013).

Despite the importance of understanding the timing of atmospheric sulphur transfer into caves, there are very few sulphur data available for karst dripwater (Wynn et al., 2008, 2010; Riechelmann et al., 2011; Tremaine and Froelich, 2013; Uchida et al., 2013). Moreover, several data are strongly modified by evapotranspiration (Tremaine and Froelich, 2013) and pyrite oxidation in the host rock (Riechelmann et al., 2011), or were collected in caves located near the sea and affected by a high proportion of sea-salt derived SO_4 (Uchida et al., 2013). Critically dripwater values were not collected close enough in time to the ca. 1975-1980 peak in anthropogenic emissions (Fig. 1) to document the

analogous succeeding peak in dripwater values.

This study aims to provide further insight into the speleothem sulphur record by reviewing the published literature and presenting new data of dripwater S concentration over time at the well-studied site of Grotta di Ernesto in Northern Italy. In particular, this paper provides the *first long-term record of sulphate concentration in cave dripwater* based on over 20 years of measurements in the cave. The dripwater data are compared with parallel data from meteoric and soil water collected over a shorter time period (2002 - 2007 AD) and with the sulphur dioxide emissions in Italy and Europe. A long-term record of S concentration is presented for a large karst spring in the region whose catchment is at high altitude and, hence, far less influenced by soil and vegetation dynamics. In this way, we aim to assess the influence of soil efficiency, vegetation cover and aquifer structure on the transmission of the S signal. By calculating an in-cave S-partition coefficient, the published S concentration data in Grotta di Ernesto ER78 stalagmite (1810 – 1998 AD; Frisia et al., 2005a, 2008) are extended to 2014 AD. The extended ER78 time series is then compared to both the S emission curves and the major historic volcanic eruptions in order to assess the transmission of the S signal under the cold temperatures and reduced soil efficiency of the Little Ice Age and under the increasing temperature, soil efficiency and S atmospheric load following industrialization. This becomes the basis for determining the transmissivity of the S signal from the atmosphere to the cave under different environmental conditions. Finally, the observed S peak of the industrial era is proposed as a relatively cheap and quick method for confirming modern calcite deposition in addition to and/or replacement of the ^{14}C-bomb peak method (Genty and Massault, 1997, 1999).

2. Sulphur in stalagmites and S cycling in forested catchments

The transmission of sulphur from atmosphere to cave dripwater and speleothems has been extensively studied at Grotta di Ernesto (ER), a mid-latitude, mid-altitude cave in the southernmost reaches of the Dolomites (Trento province, NE Italy, Fig. 2) (Fairchild et al., 2000, 2009; Frisia et al., 2005, 2008; Wynn et al., 2010, 2013). The first study of S concentration was carried out on annually laminated ER78 stalagmite and highlighted an increasing S trend from 1810 to 1998 AD interpreted as recording an increase in European S emissions through the industrial era (Frisia et al., 2005, 2008; Fairchild and Frisia, 2014). In most of the record, sulphur displayed a clear annual cyclicity, which was interpreted as related to seasonal pH changes driven by cave ventilation (Frisia et al., 2005, 2011), and independent of any seasonal variation in atmospheric S deposition (Wynn et al., 2014a). However, the 20^{th} century sulphate rise in ER78 lagged the rise in atmospheric S emissions (Fig. 1) by ca. 20 years. A similar delay was observed between peak S emissions status in Europe (1975 – 1980 AD) and the S peak in the stalagmite (1996 AD) (cf. Frisia et al., 2008). This delay was attributed to mineralisation and storage of sulphur within the soil and vegetation (eg. Wynn et al., 2013), as well as due to the hydrology of the drip site which was fed by matrix flow draining the porous portion on the aquifer and characterised by a long residence time (Miorandi et al., 2010). Critically, tree ring records of sulphur dynamics sampled from the trees above the cave demonstrated a sulphur peak which occurred earlier than in the stalagmite, thereby supporting the notion of long term storage of sulphur within the biogeochemical cycle (Fairchild et al., 2009; Wynn et al., 2014b).

The recent portion (1850 – 1996 AD) of stalagmite ER78 was subsequently analysed for sulphur and sulphur isotopes by Secondary Ionisation Mass Spectrometry by Wynn et al. (2010). The increasing trend in S concentration over the past 100 years was found to be related to the progressive incorporation of S derived from SO_2 industrial emissions, as demonstrated by sulphur isotopic composition from values close to the carbonate bedrock end-member in the pre-industrial portion, to values isotopically depleted in ^{34}S (Wynn et al., 2010). In the same study, a similar record of

143 atmospheric pollution was presented for stalagmite Obi84 from Obir cave in the Austrian Alps. Sulphur
144 in the Austrian stalagmite peaked in the 1980s and then returned toward pre-industrial levels and ^{34}S
145 enrichment in circa 10 years (Wynn et al., 2010). This suggested a less pronounced influence of
146 biogeochemical cycling and aquifer storage with respect to the ER site.

147 Isotope analysis of $\delta^{34}S\text{-}SO_4$ and $\delta^{18}O\text{-}SO_4$ were used to trace biogeochemical cycling of
148 atmospheric sulphur between 2005 and 2007 AD (Wynn et al., 2013), and highlighted that sulphate in
149 soil and dripwater at the ER site is primarily derived from an atmospheric source, while bedrock
150 contribution is only 2.1%. The weighted mean S concentration in meteoric water (423 ppb) suggested a
151 high input of sulphate derived from anthropogenic emissions, with a progressive increase in S
152 concentration in soil water (788 ppb), and cave dripwater (fast-flow st-ER1 = 1060 ppb; slow-flow st-
153 ER78 = 1350 ppb). The increase in S content in soil and dripwater with respect to the meteoric
154 signature was accompanied by a shift to higher ^{34}S values suggesting a two-phase acquisition of
155 sulphur: 1) concentration and ^{34}S-enrichment in the soil zone through storage, assimilation and
156 mineralisation; 2) S acquisition in the epikarst and in the aquifer by mixing with long residence time
157 water emplaced during times of high industrial SO_2 emissions (Wynn et al., 2013) as suggested by the
158 S trend recorded in the ER78 stalagmite (Frisia et al., 2005, 2008).

159 On the basis of the published results (Frisia et al., 2005, 2008; Wynn et al., 2010, 2013) and by
160 taking into account the different hydrology of the two drip sites (st-ER1 and st-ER78) extensively
161 studied by Miorandi et al. (2010) a conceptual model for sulphur cycling and transport at Grotta di
162 Ernesto was then developed by Wynn et al. (2013). The model identified three different scenarios (Fig.
163 3 panel A to C) and can be utilised as a reference for karst forested catchment in temperate climate
164 settings: A) under low sulphur atmospheric deposition S is biogeochemically modified by assimilation
165 and stored in the soil by mineralisation prior to entering the epikarst; B) during fast infiltration events S
166 is transmitted directly into the epikarst; C) during times of high SO_2 atmospheric deposition the relative

significance of biogeochemical cycling is diminished and most of the S is transmitted unmodified to the epikarst. In the epikarst and in the aquifer S can be rapidly transmitted into the cave via fissure flow, or stored and be subjected to redox cycling in the matrix (Fig. 3). Each drip site in the cave is characterised by a unique combination of the above conditions and the relative importance of each will vary through time as a response to changing environmental and hydrological conditions.

Critically, anthropogenic S peak was found in two stalagmites removed from two nearby caves in southwest Japan, which recorded an increase in S concentration in the course of the 20^{th} century (Uchida et al., 2013). Despite the relatively low resolution of the S record in the two Japanese samples (10 years) a clear increase of S concentration is evident after ca. 1950 AD, with peak values reached between 1990 and 2000 AD. The $\delta^{34}S$ values suggested that the S concentration peaks were related to the long-distance transport of emissions from coal burning activity in China, (Uchida et al., 2013).

3. Sulphur in stalagmites as a record of volcanic eruptions

The issue of S cycling is crucial for assessing sulphur peaks in stalagmites as markers of volcanic eruptions. In the first study highlighting S in speleothems as a proxy for volcanic eruptions, high resolution Synchrotron Radiation X-Ray Fluorescence (SR-XRF) revealed eight distinct sulphate peaks 8 to10 μm in thickness within the 5.06 to 5.19±0.16 kyr interval of stalagmite SV1 from Grotta Savi (Trieste, NE Italy) (Frisia et al., 2005). The SR-XRF map for one of the peaks demonstrated that the sulphate peak coincided with a single layer, consistent with a single seasonal input pulse, similar to the pattern of preservation of sulphate aerosol in recent ice cores (Bigler et al., 2002). Given that Grotta Savi soil is less than 50 cm thick, punctuated by rock outcrops and supporting scanty vegetation (Belli et al., 2013) the biogeochemical cycling of S likely had a minor effect. Therefore, it was hypothesized that the sulphate peaks in Grotta Savi stalagmite recorded multiple volcanic emissions (Frisia et al.,

191 2005). Similarly, SR-XRF analysis of stalagmite ER78 in the “pre-anthropogenic” period from 1810 to
192 1900 AD recorded two distinctive S peaks at circa 1815 and 1884-1888 AD, which were commensurate
193 with the ages of the Tambora (1815 AD) and Krakatau (1883 AD) eruptions (Frisia et al., 2008). Thus,
194 S- peaks in stalagmites appeared to be good candidates to mark explosive volcanic eruptions.
195 Following this assumption, a SR-XRF investigation of stalagmite So-1 (Sofular cave, Turkey)
196 was carried out with the aim of refining the age of the Minoan eruption. S concentration was shown to
197 increase above baseline levels when bromine and molybdenum peaked (at 1621 ±25 BC and 1617 ±25
198 BC respectively), whereas S peaked at 1589 ±25 BC (age model based on U/Th analyses interpolated
199 by chemical annual laminae counting) (Badertscher et al., 2014). Because Br and Mo are only
200 marginally influenced by soil and vegetation processes, their concentration peak was interpreted as
201 tracking the Minoan eruption, whilst S did not provide an accurate age of the volcanic event because it
202 had a delay of 35-40 years related to biogeochemical cycling and aquifer storage (Badertscher et al.,
203 2014). Nevertheless, the S increase above its baseline concentration is almost synchronous with the
204 peak of the “fast response” Mo and Br tracers, which suggests that S remains a reliable marker for
205 volcanism in stalagmites. The So-1 record allows hypothesizing that the Sofular karst systems was
206 characterized at the time of the eruption by a twofold response to S atmospheric signal: one, which
207 allowed the almost immediate transmission to the cave through fractures and conduits; another where
208 the S signal is delayed by biogeochemical cycling in the soil and vegetation and by aquifer storage and
209 mixing (cf. Wynn et al., 2013).
210 It is important to observe that both in Savi cave (Frisia et al., 2005, 2008) and in Sofular cave
211 (Badertscher et al., 2014) stalagmites, the peaks of S and the other “volcanogenic” elements are
212 concentrated in continuous layers, 10 to 250 μm thick. Fluorescence maps indicate that the peaks are
213 not related to micro-particle inclusions that can be incorporated within the crystal boundaries as well as
214 along the stalagmite growth surface (Frisia et al., 2005, 2012). Thus, it is important that the S

concentration peak can be related to continuous layers when claiming that the peaks are related to precise abrupt events. In this perspective, XRF microscopy should be recognized as fundamental tool in palaeoclimate research.

4. Sites description data sources and methods

The province of Trento, located within the Italian Southern Alps is characterized by mountain ranges consisting of Mesozoic carbonates, reaching elevations up to 3160 m asl, and by a large, Mesozoic carbonate karst plateau to the SE with elevation between 1000 and 2200 m asl, (Fig. 3). The valley axes cut deep through the mountains, with trends dictated by major geological structures: the N-S trending Adige Valley and the W-E trending Valsugana, which have valley bottoms at ca. 200 m asl to ca. 400 m asl respectively. The morphology of the terrain has effects on mesoscale circulation and the development of a thermal boundary layer and accumulation of pollutants dispersed from the valley bottoms during daytime heating (Gabrieli et al. 2011).

Back-trajectory studies indicate that the Trento province is mostly influenced by western Mediterranean cyclogenesis and advection of air masses from the eastern tropical Atlantic during extreme events (Bertò et al., 2004). Lagrangian moisture source diagnostic analysis (Sodemann and Zubler, 2010) revealed that the major sources of precipitation in the Southern Alps during 1995–2001 were from the western Mediterranean Sea (31%), the North Atlantic Ocean (33%), the Arctic, Nordic and Baltic Seas (13%), with the remaining 23% from land sources predominantly in the western Mediterranean, Central Europe, and the eastern North.

Grotta di Ernesto (1167 m asl, 45°58’37’’N, 11°39’28’’E) is a short and shallow (maximum rock overburden 30 m) downward gallery cut in Jurassic limestone, overlain by clay-rich calcareous brown soil (Calcari-Mollic Cambisols, pH 6.5–7.7) up to 100 cm thick. The present-day vegetation

239 above the cave is a mixed conifer - deciduous forest association, composed primarily of *Fagus*
240 *sylvatica*, *Picea abies* and *Abies alba* (Fairchild et al. 2009; Miorandi et al. 2010). Most trees started to
241 grow ca.80 years ago (Borsato et al., 2007a) following forest clearance carried out to facilitate military
242 operations before World War 1 (cf. Apolloni, 1996). This ecosystem disturbance is recorded in ER78
243 stalagmite, which shows organic-rich laminae enriched in heavy elements (Cu, Pb, Y and Zn) in the
244 period from1900 to 1920 AD, suggesting enhanced leaching of trace elements through the disturbed
245 soil profile (Borsato et al., 2007a).
246 Present day soil and aquifer dynamics at Grotta di Ernesto have been extensively investigated
247 using hydrochemistry, stable isotopes, pCO_2 and radiocarbon (Fairchild et al., 2000, Huang et al., 2001;
248 Borsato et al., 2007a; Fohlmeister et al., 2010; Frisia et al., 2010; Miorandi et al., 2010; Hartland et al.,
249 2012; Johnston et al., 2013; Borsato et al., 2015). The aquifer has a dual-permeability, with a rapid
250 fracture-flow and matrix seepage flow component feeding preferentially slow-dripping stalactites
251 (Miorandi et al., 2010). Drip rates respond to seasonal aquifer recharge, which occurs primarily during
252 the spring snowmelt (April to May) and autumn rainfall (October to November). Homogenisation of
253 the $\delta^{18}O$ and $\delta^{13}C$ signal in dripwaters contrasts with a marked seasonal signal recorded within the soil
254 water (Frisia et al., 2010). This is interpreted as mixing in the karst aquifer below the soil zone,
255 indicating a minimum mixing time of 2 years (Fohlmeister et al., 2010).
256 Acquasanta spring is one of the major karst springs of the Trento province, and its waters are
257 used for domestic consumption. Consequently, the spring has been monitored for microbiological and
258 chemical quality since 1980 (Borsato et al., 2007b; Borsato, 2010), thus representing the longest record
259 for S concentration in karst water available for the region. The resurgence opens at 477 m asl in the
260 Brenta Dolomites (46°13’00”N, 11°02’04”E), and the mean altitude of the 25 km^2 catchment is 2000 m
261 asl. A large part of the catchment is characterised by barren karst with pockets of soil supporting alpine
262 shrubs and grass and receives a mean precipitation of 1255±220 mm/year. Rainwater and snowmelt are

263 captured as both diffuse infiltration and as concentrated runoff sinking into depressions and being
264 quickly transmitted into the karst aquifer developed in a >1500 m thick Mesozoic limestone and
265 dolomite succession. Whilst the flow routes in the massive limestone are typically through fractures
266 and conduits in the dolomitic rock composed of Ca-rich dolomite with variable microstructural
267 characteristics and inter crystalline porosity (Frisia and Wenk, 1993), both matrix and fracture/conduit
268 flow are relevant. Similar to the drip regime at Grotta di Ernesto, Acquasanta spring shows strong
269 seasonal discharge variability, with high discharge recorded during snowmelt from May to June (from
270 800 to >4000 $l \cdot s^{-1}$) and low discharge in late winter and early spring (from 100 to 400 $l \cdot s^{-1}$). During the
271 highest seasonal discharge, the water mineralisation is at minimum levels, indicating a fast flow mostly
272 through conduits and large fractures, whereas in winter it displays the highest concentrations as the
273 water is drained predominantly from the smaller fissure network and the rock matrix. The Acquasanta
274 spring water should then be considered as typical for fast-response to surface changes; its high-altitude
275 catchment, above the timberline, ensures that little biogeochemical cycling of sulphur has occurred
276 from input to output of the karst waters. It is, therefore, reasonable to expect that Acquasanta waters
277 respond rapidly to the rise and decline in atmospheric S pollution levels.
278 Four dripwater sites at Grotta di Ernesto representing the two flow pathways (fracture-fed and
279 matrix-fed) were studied from 1993 to 2014. Some of the analyses from these studies have already
280 been published although often as aggregate mean values (Table 1). Drip sites st-ER77 (discharge 0.141
281 ±0.046 ml min^{-1}) and st-ER78 (discharge 0.031 ±0.035 ml min^{-1}), located 30 m below the surface and
282 0.4 m away one from each other, are slow drips, mostly fed by matrix flow. Drip sites st-ER76
283 (discharge 0.216 ±0.171 ml min^{-1}) and st-ER1 (discharge 12.4 ±11.0 ml min^{-1}), located just 20 m below
284 the surface represent intermediate (st-ER76) and fast (st-ER1) seasonal drips preferentially fed by
285 fracture flow and small conduits with a quick discharge response (less than 12 hours) to high
286 infiltration events (Miorandi et al. 2010). The time between two successive drops was measured by

287 chronometer by the same operator. The average of ten intervals for fast drips and three intervals for
288 very slow drips was then transformed into millilitres per minute by considering a mean drop volume of
289 0.12 ml, which results from measurements made on several stalactites at Grotta di Ernesto (Miorandi et
290 al. 2010).

291 Soil waters were also collected between 2002 and 2008 from two lysimeters installed above
292 Grotta di Ernesto at 0.7 m depth. From July 2004 to December 2007, bulk monthly aggregate meteoric
293 water samples from above the cave and in the meteorological station of Lavarone (30 km W of the cave
294 on the same plateau and at the same altitude) were collected by using 20 cm diameter polyethylene
295 buckets capturing both wet and dry deposition; sampling protocol and analytical details are reported in
296 Wynn et al. (2013).

297 Spring waters were collected at Acquasanta spring with different sampling frequencies.
298 Between 1987 and 1989 chemical analyses were made twice a year, few analyses were made between
299 1990 and 2002, while between 2002 and 2007 chemical analyses were made twice a year. In 2008 and
300 2009 complete chemical analyses were made on a monthly basis, whereas from 2010 to 2014 analyses
301 were made one or twice a year.

302 The dripwater, soil water and spring water samples were collected in HCl-cleaned and milli-Q®
303 water rinsed HDPE bottles. The samples were filtered with Millipore filters 0.45 μm and analysed at
304 the hydrochemistry laboratory of Istituto Agrario di San Michele all'Adige (Grotta di Ernesto) and the
305 hydrochemistry laboratory of Agenzia Provinciale per la Protezione dell'Ambiente of the Autonomous
306 Province of Trento (Acquasanta spring). The S content as well as the major ions were analysed by ion
307 chromatography following the analytical techniques described in detail in Bertoldi et al., (2011). The
308 plausibility of the results was tested against ion balance, which was better than 3% for 98% of the
309 samples.

Dripwater, soil and meteoric water at Grotta di Ernesto between 2004 and 2008 were analysed by ion chromatography at the University of Birmingham: sampling and analytical protocols are described in detail in Wynn et al., (2013).

The theoretical S-content in stalagmite ER78 for the periods 1995 – 1998, 2005 – 2008 and 2013 – 2014 AD was reconstructed by using dripwater data, and the S partition coefficient was calculated from the dripwater S/Ca ratio for the period in which the stalagmite and the dripwater series overlapped (1995-1998). For each water analysis, we utilised the mean value of 7 calcite XRF analyses corresponding to the water sampling date ± 1 month; a fixed Ca concentration of 400,000 ppm was used in account for the low concentration in other elements in the stalagmite calcite (cf. Huang et al., 2001, Borsato et al., 2007a). This approach to partitioning is an approximate solution, since Busenberg and Plummer (1985) proposed that SO_4^{2-} substitutes for CO_3^{2-} in the calcite lattice and so carbonate ion should substitute for calcium in the partition coefficient equation. This will be treated in a future publication of experimental work.

5. Results: the response of karst waters to atmospheric sulphur load

Since the beginning of the monitoring program at Grotta di Ernesto in 1993, the SO_4 concentration in dripwater has been constantly decreasing. In fast drip site st-ER1 SO_4 concentrations diminished exponentially ($R^2 = 0.84$, $p < 0.00001$) from 7.5 ±0.8 mg/l in 1993-1994 to 2.2 ±0.2 mg/l in 2013-2014 (Fig. 4). A similar exponential decrease ($R^2 = 0.92$, $p < 0.00001$) from 8.1±0.4 mg/l in 1995-1996 to 2.9 ±0.2 mg/l in 2013-2014 is evident in the slow drip sites (st-ER77, st-ER78) characterised by an overall higher SO_4 concentration with respect to fast drip st-ER1; in intermediate drip site st-ER76 the SO_4 concentration was 6.6 ±0.4 mg/l in 1995-1997. Soil water SO_4 concentration

decreased from 4.75±0.51 mg/l in 2002 to 3.74±1.58 mg/l in 2007, similar to that occurring in fast drip st-ER1.

In Acquasanta spring, water SO_4 concentration decreased slightly ($R^2 = 0.50$, $p < 0.002$) from 1.88±0.33 mg/l in 1987-1989 to 1.14 ±0.09 mg/l in 2013-2014, with a mean value of 1.46±0.37 mg/l in the years 2005 - 2006, when sulphate concentrations in meteoric water measured at Lavarone (1.35±0.62 mg/l) and Grotta di Ernesto stations (1.26±0.50 mg/l) exhibit similar values (Fig. 5). The spring water SO_4 values and the measured S content in the Mesozoic dolomites and limestones composing the Acquasanta spring aquifer (S < 270 ppm, Wynn et al., 2013), suggest the bedrock contribution to the SO_4 load is < 5% and, therefore, the S concentration in the spring water is predominantly related to the atmospheric input.

6. Discussion

6.1. Sources of S emissions

Available SO_4 analyses for other karst spring waters of the same region with catchments above 2000 m asl and aquifers developed in similar lithology, show sulphate levels and trends similar to those recorded for Acquasanta spring for the last 10 years (Borsato, 2010). However, dripwater in other caves in the southern part of the Trento province (cf. Fig. 2) exhibit similar, or higher, SO_4 concentration with respect to Grotta di Ernesto. During the period 2002-2003, dripwater SO_4 concentration in the mid altitude Giazzera cave (infiltration elevation 1050 m asl) was 4.9 ± 0.2 mg/l, whereas in the low altitude Bus del Diaol cave (infiltration elevation 355 m asl) was 9.4 ± 0.8 mg/l (Borsato et al., submitted). This spatial heterogeneity with respect to the infiltration elevation and latitude is similar to that observed in the chemistry of surface snow in the same region, where the lowest concentrations in

357 SO_4 and other trace elements were measured in snow collected above 2000 m asl in the northernmost
358 part of the Trento province, and the highest concentrations in snow at mid and low elevations in the
359 southernmost reaches of the studied area (Gabrielli et al., 2008; Gabrieli et al., 2011). This suggests
360 that, in addition to sea-salt, aeolian dust and bedrock contributions, there are two other factors that need
361 to be accounted for when interpreting S concentration in meteoric and karst water: the geographic
362 location relative to sources of S emissions and the altitude of the boundary layer.
363 The latitudinal trend in cave drips, karst spring water and snow can be ascribed to their relative
364 proximity to the highly industrialized Po Valley and Venetian Plain towards the South and East (Fig.
365 3), the most important regional sources of anthropogenic S pollution. This is confirmed by similar
366 observations made in the southern watershed of the central Alps where a clear South to North
367 diminishing trend in the SO_4 atmospheric deposition was documented (Rogora et al., 2006).
368 On the other hand, the decrease in SO_4 concentration with respect to site elevation is related to the
369 position of the local boundary layer (Gabrielli et al., 2008; Gabrieli, 2011). Balloon data from the
370 meteorological station of Milano-Linate (in the Po Valley, 190 km WSW of Grotta di Ernesto) indicate
371 that, in winter, the boundary layer depth (BLD) is higher than 2000 m asl only for a very limited
372 amount of time (15 to 20%), whereas a well-mixed boundary layer exists below 500 m asl (Gabrieli et
373 al. 2011). Therefore, in winter, the pollutants released in the Po Valley and Venetian Plain, as well as
374 on the western and northern side of the Alps, are confined to the lower elevation belt (i.e. Bus del
375 Diaol). The BLD rises in summer, due to stronger insolation that results in more effective convection,
376 and it is higher than 2000 m asl for 72% of the days from April to September (Gabrieli et al. 2011).
377 This allows the pollutants to be lifted and transported horizontally by the synoptic flow across the Alps
378 (Gabrieli et al., 2011). A similar consideration holds true for the western Alps, where the S atmospheric
379 concentration measured in 1991-1993 increased up to two orders of magnitude from low elevation sites
380 (500 m asl) to the highest glacier site (Col du Dôme, French Alps, 4250 m asl). Accordingly, from

1975 to 1985 AD, the summer S concentration in the Col du Dôme ice core was four times higher than the winter value (Preunkert et al., 2001).

The variability in altitude of the local boundary layer influences the input of atmospheric S, and explains the greater contribution of anthropogenic sulphate in the southernmost sites (nearer to the local S-emissions) and at lower elevations. It is then reasonable to assume that caves at mid altitude in industrialized regions would record the effects of BLD variability, in addition to a regional atmospheric S signal modified by ecosystem and aquifer processes.

In assessing the provenance of anthropogenic emissions, the synoptic setting must be considered. By using the aforementioned contribution to the sources to precipitations in the Southern Alps (Sodemann and Zubler, 2010), the emissions affecting the study area over time were calculated. Tabulated emissions are available for different European countries (Mylona, 1996, 1997; Vestreng et al., 2007) and these were combined in the proportions: Italy (proximal location, 50% contribution), Spain and France (North Atlantic region, 36%), and finally Germany, Poland, Hungary and Czech Republic (northern provenance, 14%). As expected, the resulting emission curve is similar to the total European emission curve, although the regional emission curve has a narrower peak that accounts of the more pronounced contribution from Italy (Fig. 1).

6.2. The industrial era S peak, aquifer storage and dilution effect

SO_2 emissions associated with the industrial era and enhanced in 1950 – 2000 AD (Fig. 1) and their fallout in karst soils can be considered as a global "tracing test" for caves around the world, similar to the effects of the ^{14}C bomb peak produced by nuclear tests during the 1960s (Genty and Massault, 1999). This is particularly true for caves developed in almost pure carbonate rocks where the S content in the host-rock is very low and the S in dripwater is derived almost entirely from

405 atmospheric sources (cf. Cap. 1). In these contexts the dynamics of sulphur emissions to the
406 atmosphere will be replicated within cave drip and karstic groundwater according to the variable extent
407 of biogeochemical cycling, water residence time and the degree of water source mixing. Waters
408 emerging at Aquasanta spring, where there has been little to no retention in the biogeochemical cycle
409 and hydrology is dominated by conduits and fracture flow, display sulphur concentrations closely
410 aligned to immediate atmospheric SO_2 loading (Figure 5).
411 At Ernesto cave, where the retention in the biogeochemical cycling is relevant, the dripwater
412 composition should be more influenced by past atmospheric composition and, by considering that SO_2
413 emissions in the atmosphere are constantly decreasing following peak emissions status in 1976 AD
414 (Fig. 1), we can expect an higher S content in dripwater with respect to the coeval atmospheric SO_2
415 loading (Figure 5). For the same reason, drip sites fed predominantly by matrix flow (st-ER77 and st-
416 ER78) support concentrations of sulphur which are greater than those drip sites fed by fracture flow
417 dynamics (st-ER76 and st-ER1) in relation to the higher proportion in matrix fed stalactites of older
418 water with respect to fissure fed sites characterised by a shorter residence time.
419 In the case of drips st-ER76 and st-ER1 fed preferentially by fast fissure flow but with a
420 component of matrix flow (Miorandi et al., 2010) a dilution effect can be expected during higher
421 discharge periods, characterized by a major contribution of fast flow through fissures and conduits and
422 a reduced contribution from older water with high S-content stored in the aquifer. This is illustrated in
423 Fig. 6A, where the SO_4 concentration in fast-drip st-ER1 during specific time intervals (to minimize the
424 influence of the progressive decrease in time of the SO_4 concentration in the aquifer matrix) displays a
425 negative exponential correlation with discharge. In particular, the SO_4 concentration varies from a high
426 concentration end-member corresponding to the contribution from the porous matrix to a low
427 concentration end-member reflecting the mean composition in the epikarst fractures, and similar to the
428 mean soil water concentration (Fig. 6A). By contrast, for the slow drip sites st-ER77 and st-ER78,

where the fissure flow component is negligible, no correlation between water SO_4 concentration and discharge is evident (Fig. 6B).

Finally, by comparing the trends in the S series we can observe an offset of about 4.5 years between st-ER78 (matrix flow) and st-ER1 (predominant fissure flow) (Fig. 4 and A1). This time span should represent the additional delay related to the S retention in the aquifer matrix, although additional variables such as the different flow path of the two drips, the possible S-concentration related to the sulphate reduction in the aquifer and the secondary contribution from the host-rock must be taken into account.

6.3. Sulphur trend in stalagmite ER78

Annually laminated calcite stalagmite ER78 (Frisia et al., 2003), fed by stalactite st-ER78, was analysed by synchrotron radiation X-ray fluorescence (XRF) at 2µm resolution (corresponding to ~32 analyses/year for the last century). The measured intensities (counts per seconds) could not be transformed in actual concentrations because of the lack of standards with similar matrix (Frisia et al., 2005). The successive analyses by Secondary Ionisation Mass Spectrometry (SIMS) of the topmost part of the stalagmite (Wynn et al., 2010) allowed quantification of the synchrotron XRF data (Fig. A2). In Fig. 7 the quantified S data and the lamina thickness of ER78 are compared with the surface temperature record, the S emission trend as well as with the SO_4 record in the Alpine ice core at Col du Dôme (Preunker et al., 2001).

When considering the characteristic S emission peak from 1950 to 2010 AD, centred at 1976 AD, a delay of ca. 20 years can be observed in both the rising limb of the S series and the maximum value (1996 AD). As discussed above, stalactite st-ER78 is fed by matrix flow with little contribution from fast fissure flow. Thus, the S concentration in ER78 stalagmite is expected to reflect the S

composition in the epikarst and in the vadose zone (Wynn et al., 2013). Therefore, in the present-day situation of relatively low sulphur atmospheric deposition, S is biogeochemically modified in the soil prior to entering the epikarst (scenario A in Fig.3). The 20-year delay for the transmission of the atmospheric S signal to ER78 stalagmite, thus represents the sum of biogeochemical cycling and aquifer storage. However, the biogeochemical cycling of sulphur above the cave may not always have operated to similar extent, dependent upon vegetation density, soil efficiency and levels of sulphur loading to the overlying ecosystem.

During the cold Little Ice Age in the 19th century, temperatures in Northern Italy were significantly lower than the mean 20th century values (-0.98±0.2°C calculated at Milan between 1800 – 1880 with respect to the 1901-1995 reference period; Maugeri and Nanni, 1998, Fig. 7). Cooling was more pronounced than the value calculated for the European Alps and the rest of Europe (-0.33±0.1°C, Luterbacher et al., 2004; Casty et al., 2005) and was likely responsible for the reduced annual growth rate of stalagmites in Grotta di Ernesto (Frisia et al., 2003). Stalagmite growth rate (measured as annual lamina thickness) depends on a number of factors including temperature, drip-rate, dripwater Ca content, fluid film thickness, cave air pCO_2 (Dreybrodt, 1999) and the presence of growth inhibitors (Meyer, 1984; Frisia et al., 2012). Of these, variations in drip-water supersaturation due to Ca content or drip water pCO_2 (as a function of degassing in the epikarst or in the cave) are the most likely to vary on a multi-year timescale (Frisia et al., 2003). These factors control parent water supersaturation with respect to calcite, and reflect changes in CO_2 production and storage in the soil and epikarst above the cave. In the studied area, these processes are modulated by temperature (Borsato et al., 2015). A decrease of 1°C in the mean annual temperature would cause a decrease of 0.1 in the calcite saturation index (SI_{CC}) (Borsato et al., 2015) and this, by considering the present-day saturation in ER dripwater (SI_{CC} = 0.38±0.15, Miorandi et al., 2010) would result in significant reduction in the stalagmite growth rate (Dreybrodt, 1999; Frisia et al., 2003). Cooling also results in a reduction of vegetation cover and

soil activity (Frisia et al., 2003; Borsato et al., 2015) by slowing the biogeochemical cycling above the cave (scenario C in Fig. 3). Diminished soil efficiency during the Little Ice Age is also testified by the presence of thin (1-4 μm), brown UV-luminescent, organic and trace element-enriched sub-laminae at the beginning of each hydrological year in autumn (Frisia et al., 2003; Borsato et al., 2007a; Scholz et al., 2012). This suggests that microbial decomposition of organic matter in the soil zone was not as efficient as in the 20^{th} century, when organic-rich sub-laminae almost disappear. Under these circumstances, any delay in transmitting an atmospheric S signal to the cave was probably reduced to a few years. This may explain why the volcanic eruptions of 1815 and 1883 AD were recorded as narrow and short-term (4-6 years) S spikes, with apparently little delay or modification of the atmospheric signal (Fig. 7).

Starting from 1900 AD, the annual growth rate of ER78 increased, following temperature and solar radiation increase. A high sensitivity of the site to solar radiation is confirmed by spectral density at the 11 year solar cycle recorded by the lamina thickness series (Frisia et al., 2003). Higher temperature resulted in higher soil pCO_2 production (Borsato et al., 2015), more efficient host rock dissolution leading to higher Ca^{2+} content in cave waters (Dreybrodt, 1999) and, ultimately, to faster growth rate in Grotta di Ernesto stalagmites (Frisia et al., 2003; Smith et al., 2006). Critically, the increase in solar radiation and surface temperature coincided with industrialization, and a steady rise in S emissions from 1890 to 1940 (Fig. 7). From 1950 there was a steep increase in S emissions, which lasted until 1980, and an equally steep decline after that. These features are reproduced with a variable delay by the S trend in ER78 likely related to the increasing vegetation cover and soil efficiency that enhanced S biogeochemical cycling through the uptake and assimilation of sulphate in plants and soil/root microorganisms, and S mineralisation and storage in the soil zone. In addition, the combination of warming plus increasing pollution levels resulted in variations in BLD, which reached the mid altitudes throughout the warm season, causing an enhanced transport of the S-emissions over

the Italian Alps at mid altitudes. A constant, high supply of atmospheric S eventually overcame the S biogeochemical cycling capacity, thus, a significant proportion of atmospheric S was transmitted, unmodified to the epikarst (scenario C in Fig. 3). Following these considerations, it is reasonable to infer that ER78 stalagmite captured atmospheric S emissions with limited delay before the 20th century warming. This explains why pre-1900 explosive volcanic eruptions are recorded by well-defined, short-lived S peaks in the stalagmite record as highlighted by the detrended S concentration (Fig. 7).

In the same detrended series between 1890 and 1970, when both lamina thickness and S content commenced to increase, it is possible to observe a marked annual structure related to seasonal fluctuations of dripwater pCO_2 driven by cave ventilation (Frisia et al., 2011; Wynn et al., 2014a). Starting from 1970, the S structure becomes noisy, and the annual signal is complicated by secondary peaks, most likely in relation to high S flux from the soil zone, and the mixing in the aquifer of different sources characterised by different S content (Fig. 3).

6.4. A future projection of the ER78 sulphur series and the anthropogenic S-peak

The S concentrations in stalagmite ER78 and dripwater analyses for the corresponding drip site st-ER78, allow for the calculation of the S partition coefficient (D_S) for the period in which the two series overlapped (1995-1998):

$$\textit{Partition coefficient: } D_S = \frac{\frac{S}{Ca}\,stalagmite}{\frac{S}{Ca}\,dripwater}$$

523 The calculated D_S for each single water analysis are plotted against their corresponding S/Ca
524 ratio in the inset of Fig. 8, where a linear relationship between the calculated D_S and the dripwater S/Ca
525 ratio can be observed:
526
527 D_S = 0.148 S/Ca (molar) - 0.01 (R^2 = 0.82, p < 0.0005);
528
529 By using the mean calculated D_S value (D_S = 0.0064 ± 0.10; cf. inset in Fig. 8) the theoretical
530 stalagmite S content from the dripwater S/Ca data is reconstructed, and used to complement the sulphur
531 record in stalagmite ER78 (Fig. 9). The exponential decrease evidenced by dripwater S/Ca data (R^2 =
532 0.89, p < 0.0001, Fig. 8) can then be used to project a theoretical stalagmite S-content up to 2030 AD,
533 when the predicted values should reach pre-industrial values (around 15 ppm).
534 The reconstructed stalagmite series can then be compared with the SO_2 emissions: both series
535 are characterised by a prominent peak lasting 70-80 years and with values up to 10-15 times the pre-
536 industrial concentration (Fig. 9). The rising limb and the centre of the S peak in the stalagmite are
537 delayed by ~20 years with respect to the S-emission peak, which is explained by biogeochemical
538 cycling and aquifer storage. By contrast, it is difficult to evaluate the delay in the more recent part of
539 the series because there are no equivalent points identifiable in the falling limb between the emissions
540 and the speleothem time series. However, by considering that the emissions in 2005 decreased to levels
541 similar to the 1920s levels and that the projected speleothem values should reach the corresponding
542 levels around 2025, we can estimate a similar delay of ~20 years. The stalagmite peak in its central
543 part (1990 – 2000) is sharper that the corresponding emissions peak: here we suggest that this can be
544 related to the transmission of part of the atmospheric S load unmodified into the epikarst, following the
545 overload in the soil and ecosystem above the cave (scenario C in Fig. 3).

546 On the basis of these considerations, the delay in sulphur transmission between atmosphere and
547 stalagmite ER78 can be divided into three characteristic periods: i) in the pre-industrial era and the first
548 part of the 20th century the delay was of few years (possibly 4 to 8 years and mostly related to the mean
549 residence time in the aquifer) as the biogeochemical cycling was not very efficient; ii) starting from
550 1950 AD following the establishment of the forest above the cave and the enhanced atmospheric S
551 load, the delay progressively increased up to 20 years; iii) the increasing atmospheric S deposition
552 caused an "overload" in the soil and ecosystem above the cave, allowing the transmission of part of the
553 atmospheric S unmodified into the epikarst and sharpening the stalagmite peak in its central part (Fig.
554 9).
555 The anthropogenic S-peak is a very prominent feature in ER78 stalagmite, as well as in the
556 record from Austrian stalagmite Obi84 (Wynn et al., 2010) and in two Japanese stalagmites (Uchida et
557 al., 2013). Therefore, it can be used in speleothem-based palaeoclimate research to refine modern
558 chronology and acquire complementary information regarding the soil and vegetation biogeocycling
559 efficiency through time. In ideal cases, the S record can be characterized by an annual signal related to
560 seasonal fluctuations of dripwater pCO_2 (Frisia et al., 2011; Wynn et al., 2014a) that can be used to
561 further refine speleothem chronology.
562 The anthropogenic S-peak is complementary to the ^{14}C bomb peak, which is used to date the
563 modern portion of speleothems (Genty and Massault, 1999; Mattey et al., 2008). With respect to the S-
564 peak, the ^{14}C bomb peak has the advantage of an initial rise around year 1958, which provides a
565 reliable marker for dating and correlation (Hodge et al., 2014). However, the maximum ^{14}C peak in
566 speleothems can be lagged by up to 20 years with respect to the atmospheric peak centred at circa
567 1965, and the stalagmite signal can be affected by differing degrees of attenuation. Notwithstanding,
568 the major disadvantage is the technical aspect of the analyses, which are destructive, expensive and
569 time consuming. By contrast, recent advances of the sulphur analytical techniques such as SR-XRF,

570 SIMS and high mass resolution ICP mass spectrometry (Jochum et al., 2012) are now opening new
571 avenues of approach and we foresee that high resolution analyses of S concentration in recent
572 speleothems will be routinely carried out in future palaeoclimate reconstructions.
573
574
575 **8. Conclusions**
576
577 S concentration variability in stalagmites represents a valuable proxy for volcanic eruptions and
578 anthropogenic emissions, and it may potentially become a highly sensitive proxy for high resolution
579 palaeoclimate and palaeoenvironmental reconstructions.
580 The study of soil processes and aquifer dynamics, as well as the knowledge of the synoptic
581 setting and geographic location with respect to emissions source, is an important pre-requisite for
582 successful interpretation of speleothem S series. Variations in the background levels of sulphur
583 contained within speleothems and the shape and duration of S peaks in both Holocene and pre-
584 Holocene stalagmites, especially when used in conjunctions with other trace elements, are able to
585 provide indications about changes in rates of biogeochemical cycling, as well as independent
586 information on the contribution of volcanic processes to atmospheric load. Moreover, when analysed at
587 high temporal resolution, annual cycles in the S record can be used to complement the dating accuracy
588 and the seasonality information gained from other more traditionally studied elements, such as Mg and
589 Sr (Fairchild and Treble, 2009; Badertscher et al., 2014).
590 Eventually, the potential of sulphur in speleothems as marker of volcanic eruptions (and,
591 consequently, as a correlative tool) depends on ecosystem biogeochemical cycling and mean residence
592 time of the water in the aquifer. Where signals in speleothem calcite are reliant on passing from
593 atmosphere to cave via the sulphur biogeochemical cycle, we suggest the best locations to obtain

accurate records of past volcanic eruptions from speleothems are mid altitude, and high to mid latitude caves sites with thin soil cover and highly transmissive aquifers. Tropical and equatorial caves with thick soil cover and long water residence time are the worst candidates. However, speleothems from tropical and equatorial settings formed in caves cut in pure carbonate rocks overlain by scanty soils, or characterized by high-rockiness soils, where aquifers are highly transmissive could yield a reliable volcanic record. S should be used in conjunction with other volcanogenic trace elements such as Br and Mo and high resolution mapping techniques could also be useful in order to distinguish thin continuous layers from discrete grain inclusions.

Industrial anthropogenic SO_2 emissions can be considered a global "tracing test" for dripwater and groundwater in the Northern Hemisphere. In this perspective Grotta di Ernesto is particularly apt to capture the anthropogenic S emissions, being near the Venetian Plain, one of the most industrialized areas in Italy. Despite the delay in the transfer of the atmospheric signal from surface to cave, it is here demonstrated that the anthropogenic S peak is well preserved in both dripwater and speleothems. Thus, it is here proposed the use of the anthropogenic S concentration peak as an additional dating tool for recent speleothems, complementary to the radiocarbon bomb peak.

Acknowledgements:

The monitoring at Grotta di Ernesto was carried out within the framework of the AQUAPAST Project funded by the Autonomous Province of Trento (Italy), and the DFG Research Group 668 DAPHNE Project, funded by Deutsche Forschungsgemeinschaft (Germany). PW would like to thank the UK Natural Environment Research Council (NERC) for funding part of this work (Grant NE/C511805/1). We thank Dr. Flavio Corradini (Hydrochemistry Laboratory of Istituto Agrario di San Michele

all'Adige, Trento) for part of the analyses at Grotta di Ernesto. The Acquasanta spring analyses were kindly provided by *Servizio Geologico* (Geological Survey) and *Agenzia Provinciale per la Protezione dell'Ambiente* of the Autonomous Province of Trento. Thanks are also expressed to Michele Zandonati (Museo Tridentino di Scienze Naturali, Trento) for logistical support at Grotta di Ernesto.

References

Badertscher, S., Borsato, A., Frisia, S., Berger, A., Gokturk, O., Fleitmann, D., 2014. Santorini eruption recorded in a stalagmite from Sofular Cave, Northern Turkey. Earth and Planetary Science Letters 392, 58-66.

Belli, R., Frisia, S., Borsato, A., Drysdale, R., Hellstrom, J., Zhao, J.X., Spötl, C., 2013. Regional climate variability and ecosystem responses to the last deglaciation in the northern hemisphere from stable isotope data and calcite fabrics in two northern Adriatic stalagmites. Quaternary Science Reviews 72, 146-158.

Bertoldi, D., Bontempo, L., Larcher, R., Nicolini, G., Voerkelius, S., Lorenz, G.D., Ueckermann, H., Froeschl, H., Baxter, M.J., Hoogewerff, J., Brereton, P., 2011. Survey of the chemical composition of 571 European bottled mineral waters. Journal of Food Composition and Analysis 24, 376-385.

Bertò, A., Buzzi, A., Zardi, D., 2004. Back-tracking water vapour contributing to a precipitation event over Trentino: A case study. Meteorologische Zeitschrift 13, 189-200.

Bigler, M., Wagenbach, D., Fischer, H., Kipfstuhl, J., Miller, H., Sommer, S., & Stauffer, B. 2002. Sulphate record from a northeast Greenland ice core over the last 1200 years based on continuous flow analysis. Annals of Glaciology, 35(1), 250-256.

642 Borsato, A., 2010. Monitoraggio idrogeologico e geochimico del massiccio del Brenta.
643 (*Hydrogeological and geochemical monitoring of Brenta Dolomites massif*). Servizio Geologico
644 Provincia Autonoma di Trento, 242 pp.
645 Borsato, A., Frisia, S., Fairchild, I.J., Somogyi, A., & Susini, J., 2007a. Trace element distribution in
646 annual stalagmite laminae mapped by micrometer-resolution X-ray fluorescence: implications for
647 incorporation of environmentally significant species, Geochimica et Cosmochimica Acta 71,
648 1494–1512.
649 Borsato, A., Frisia, S., Van der Borg, K., 2007b. Present-day and Holocene groundwater fluctuations in
650 Bus de la Spia – Acquasanta karst system and their impact on the formation of hypogean
651 calcareous tufa. Proceedings XXXV Congress International Association of Hydrogeologists –
652 Groundwater and Ecosystem, Lisbon 2007, p. 4.
653 Borsato, A., Johnston, V.E., Frisia, S., Miorandi, R., Corradini, F., (submitted). Altitudinal trend and
654 seasonal variability of cave dripwater chemistry and implications for speleothem-based
655 palaeoclimate studies. Geochimica et Cosmochimica Acta (submitted for publication).
656 Borsato, A., Frisia, S., Miorandi, R. 2015. Carbon dioxide concentration in temperate caves and parent
657 soils over an altitudinal gradient: implications for speleothem growth rates and fabrics. Earth
658 Surface Processes and Landforms. DOI: 10.1002/esp.3706
659 Busenberg, E. & Plummer, L.N. 1985. Kinetic and thermodynamic factors controlling the distribution
660 of SO_4^{2-} and Na^+ in calcites and selected aragonites. Geochimica et Cosmochimica Acta 49, 713-
661 725.
662 Casty, C., Wanner, H., Luterbacher, J., Esper, J., Böhm, R., 2005. Temperature and precipitation
663 variability in the European Alps since 1500. International Journal of Climatology 25, 1855-1880.
664 Dreybrodt, W., 1999. Chemical kinetics, speleothem growth and climate. Boreas 28, 347-356.

European Environmental Agency, 2014: http://www.eea.europa.eu/data-and-maps/indicators/eea-32-sulphur-dioxide-so2-emissions-1/assessment-3. (accessed on December 2014).

Fairchild, I.J., Borsato, A., Tooth, A.F., Frisia, S., Hawkesworth, C.J., Huang, Y., McDermott, F. and Spiro, B. 2000. Controls on trace element (Sr-Mg) compositions of carbonate cave waters: implications for speleothem climatic records. Chemical Geology, 166, 255-269.

Fairchild, I.J., Loader, N.J., Wynn, P.M., Frisia, S., Thomas, P.A., Lageard, J.G.A., de Momi, A., Hartland, A., Borsato, A., La Porta, N., & Susini, J., 2009. Sulfur Fixation in Wood Mapped by Synchrotron X-ray Studies: Implications for Environmental Archives. Environ. Sci. Technol., 43 (5), 1310-1315.

Fairchild, I.J., Treble, P.C., 2009. Trace elements in speleothems as recorders of environmental change. Quaternary Science Review 28, 449-468.

Fohlmeister, J., Schröder-Ritzrau, A., Spötl, C., Frisia, S., Miorandi, R., Kromer, B., Mangini, A., 2010. The influences of hydrology on the radiogenic and stable carbon isotope composition of cave drip water, Grotta di Ernesto (Italy). Radiocarbon 52, 1529-1544.

Frisia, S., Borsato, A., Fairchild, I.J., Susini J., 2005. Variations in atmospheric sulphate recorded in stalagmites by synchrotron micro XRF and XANES analyses. Earth and Planetary Science Letters 235, 729-740.

Frisia, S., Borsato, A., Preto, N., McDermott, F., 2003. Late Holocene annual growth in three Alpine stalagmites records the influence of solar activity and the North Atlantic Oscillation on winter climate. Earth and Planetary Science Letters 216, 411-424.

Frisia, S., Borsato, A., & Susini, J., 2008. Synchrotron radiation applications to past volcanism archived in speleothems: An overview. Journal of Vulcanology and Geothermal Research 177, 1, 96-100.

688 Frisia, S., Wenk, H.R., 1993. TEM and AEM study of pervasive multi-step dolomitization of the Upper
689 Triassic Dolomia Principale (northern Italy). Journal of Sedimentary Petrology 63, 1049-1058.
690 Gabrielli, P., Cozzi, G., Torcini, S., Cescon, P., Barbante, C., 2008. Trace elements in winter snow of
691 the Dolomites (Italy): A statistical study of natural and anthropogenic contributions.
692 Chemosphere 72, 1504-1509.
693 Gabrieli, J., Carturan, L., Gabrielli, P., Kehrwald, N., Turetta, C., Cozzi, G., Spolaor, A., Dinale, R.,
694 Staffler, H., Seppi, R., 2011. Impact of Po Valley emissions on the highest glacier of the Eastern
695 European Alps. Atmospheric Chemistry and Physics 11, 8087-8102.
696 Genty, D., Massault, M,. 1997. Bomb ^{14}C recorded in laminated speleothems: calculations of dead
697 carbon proportion. Radiocarbon 39(1):33–48.
698 Genty, D., Massault, M., 1999. Carbon transfer dynamics from bomb-^{14}C and $\delta^{13}C$ time series of a
699 laminated stalagmite from SW France—Modelling and comparison with other stalagmite records.
700 Geochimica et Cosmochimica Acta 63, 1537-1548.
701 Hartland, A., Fairchild, I.J., Lead, J.R., Borsato, A., Baker, A., Frisia, S., Baalousha, M., 2012. From
702 soil to cave: Transport of trace metals by natural organic matter in karst dripwaters. Chemical
703 Geology 304–305, 68-82.
704 Hodge, E., McDonald, J., Fischer, M., Redwood, D., Hua, Q., Levchenko, V., Drysdale, R., Waring,
705 C., Fink, D., 2011. Using the 14 C bomb pulse to date young speleothems. Radiocarbon 53, 1-13.
706 Huang, Y., Fairchild, I.J., Borsato, A., Frisia, S., Cassidy, N.J., McDermott, F., Hawkesworth, C.J.,
707 2001. Seasonal variations in Sr, Mg and P in modern speleothems (Grotta di Ernesto, Italy).
708 Chemical Geology 175, 429-448.
709 Jochum, K.P., Scholz, D., Stoll, B., Weis, U., Wilson, S.A., Yang, Q., Schwalb, A., Börner, N., Jacob,
710 D.E., Andreae, M.O., 2012. Accurate trace element analysis of speleothems and biogenic calcium
711 carbonates by LA-ICP-MS. Chemical Geology 318–319, 31-44.

712 Johnston, V.E., Borsato, A., Spötl, C., Frisia, S., Miorandi, R., 2013. Stable isotopes in caves over
713 altitudinal gradients: Fractionation behaviour and inferences for speleothem sensitivity to climate
714 change. Climate of the Past 9, 99-118.
715 Legrand, M., Mayewski, P., 1997. Glaciochemistry of polar ice cores: a review. Reviews of geophysics
716 35, 219-243.
717 Likens, G.E., Driscoll, C.T., Buso, D.C., Michell, M.J., Lovett, G.M., Bailey, S.W., Siccama, T.G.,
718 Reiners, W.A. and Alewell, C. 2002. The Biogeochemistry of sulphur at Hubbard Brook.
719 Biogeochemistry 50, 235 – 316.
720 Luterbacher, J., Dietrich, D., Xoplaki, E., Grosjean, M., Wanner, H., 2004. European seasonal and
721 annual temperature variability, trends, and extremes since 1500. Science 303, 1499-1503.
722 Mattey, D., Lowry, D., Duffet, J., Fisher, R., Hodge, E., Frisia, S., 2008. A 53 year seasonally resolved
723 oxygen and carbon isotope record from a modern Gibraltar speleothem: Reconstructed dripwater
724 and relationship to local precipitation. Earth and Planetary Science Letters 269, 80-95.
725 Mayewski, P., Lyons, W., Spencer, M., Twickler, M., Dansgaard, W., Koci, B., Davidson, C., Honrath,
726 R., 1986. Sulfate and nitrate concentrations from a south Greenland ice core. Science 232, 975-
727 977
728 Maugeri, M., Nanni, T., 1998. Surface air temperature variations in Italy: recent trends and update to
729 1993, Theoretical and Applied Climatology 61, 191-196.
730 McDermott, F., 2004. Palaeo-climate reconstruction from stable isotope variations in speleothems: a
731 review. Quaternary science review 23, 901-918.
732 Meyer, H.J., 1984. The influence of impurities on the growth rate of calcite. Journal of Crystal Growth
733 66, 639-646.

734 Miorandi, R., Borsato, A., Frisia, S., Fairchild, I.J. & Richter, D.K., 2010. Epikarst Hydrology and
735 implications for stalagmite capture of climate changes at Grotta di Ernesto (N.E. Italy): results
736 from long-term monitoring. Hydrological Processes. 24, 3101–3114.
737 Mylona, S. 1996. Sulphur dioxide emissions in Europe 1880–1991, Tellus, 48B, 662–689, ISSN 0280-
738 6509.
739 Mylona, S. 1997. Corrigendum to Sulphur dioxide emissions in Europe 1880–1991, Tellus, 49B, 447–
740 448, ISSN 0280-6509.
741 Neftel, A., Beer, J., Oeschger, H., Zürcher, F., Finkel, R., 1985. Sulphate and nitrate concentrations in
742 snow from South Greenland 1895–1978. Nature 314, 611 - 613.
743 Novak, M., Mitchell, M.J., Jackova, I., Buzek, F., Schweigstillova, J., Erbanova, L., Prikryl, R.,
744 Fottova, D., 2007. Processes affecting oxygen isotope ratios of atmospheric and ecosystem
745 sulphate in two contrasting forest catchments in central Europe. Environmental Science and
746 Technology 41, 703 – 709.
747 Patris, N., Delmas, R., Legrand, M., De Angelis, M., Ferron, F.A., Stiévenard, M., Jouzel, J., 2002.
748 First sulfur isotope measurements in central Greenland ice cores along the preindustrial and
749 industrial periods. Journal of Geophysical Research: Atmospheres (1984–2012) 107, ACH 6-1-
750 ACH 6-11.
751 Preunkert, S., Legrand, M., Wagenbach, D., 2001. Sulfate trends in a Col du Dome (French Alps) ice
752 core: A record of anthropogenic sulfate levels in the European midtroposphere over the twentieth
753 century. Journal of Geophysical Research: Atmospheres (1984–2012) 106, 31991-32004.
754 Riechelmann, D.F.C., Schröder-Ritzrau, A., Scholz, D., Fohlmeister, J., Spötl, C., Richter, D.K.,
755 Mangini, A., 2011. Monitoring Bunker Cave (NW Germany): A prerequisite to interpret
756 geochemical proxy data of speleothems from this site. Journal of Hydrology 409, 682-695.

Rogora, M., Mosello, R., Arisci, S., Brizzio, M., Barbieri, A., Balestrini, R., Waldner, P., Schmitt, M., Stähli, M., Thimonier, A., 2006. An overview of atmospheric deposition chemistry over the Alps: present status and long-term trends. Hydrobiologia 562, 17-40.

Scholz, D., Frisia, S., Borsato, A., Spötl, C., Fohlmeister, J., Mudelsee, M., Mühlinghaus, C., Miorandi, R., Mangini, A., 2012. Holocene climate variability in north-eastern Italy: potential influence of the NAO and solar activity recorded by speleothem data. Climate of the Past 8, 1367–1383.

Schwikowski, B.M., Döscher, A., Gäggeler, H., Schotterer, U., 1999. Anthropogenic versus natural sources of atmospheric sulphate from an Alpine ice core. Tellus B 51, 938-951.

Shanley, J.B., Mayer, B., Mitchell, M.J., Michel, R.L., Bailey, S.W., Kendall, C., 2005. Tracing sources of streamwater sulphate using S and O isotope ratios of sulphate and ^{35}S activity. Biogeochemistry 76, 161 – 185.

Smith, C.L., Baker, A., Fairchild, I.J., Frisia, S., Borsato, A., 2006. Reconstructing hemispheric-scale climates from multiple stalagmite records. International Journal of Climatology 26, 1417-1424.

Sodemann, H., Zubler, E,. 2010. Seasonal and inter-annual variability of the moisture sources for Alpine precipitation during 1995–2002. International Journal of Climatology 30, 947–961.

Tremaine, D.M., Froelich, P.N., 2013. Speleothem trace element signatures: A hydrologic geochemical study of modern cave dripwaters and farmed calcite. Geochimica et Cosmochimica Acta 121, 522-545.

Uchida, S., Kurisaki, K., Ishihara, Y., Haraguchi, S., Yamanaka, T., Noto, M., Yoshimura, K., 2013. Anthropogenic impact records of nature for past hundred years extracted from stalagmites in caves found in the Nanatsugama Sandstone Formation, Saikai, Southwestern Japan. Chemical Geology 347, 59-68.

Vestreng, V., Myhre, G., Fagerli, H., Reis, S and Tarrasón, L. 2007. Twenty-five years of continuous sulphur dioxide emission reduction in Europe. Atmospheric Chemistry and Physics 7, 3663-3681.

781 Wagenbach, D., Münnich, K., Schotterer, U., Oeschger, H., 1988. The anthropogenic impact on snow
782 chemistry at Colle Gnifetti, Swiss Alps. Ann. Glaciol 10, 183-187.
783 Wynn, P.M., Fairchild, I.J., Baker, A., Baldini, J.U., McDermott, F., 2008. Isotopic archives of
784 sulphate in speleothems. Geochimica et Cosmochimica Acta 72, 2465-2477.
785 Wynn, P.M., Fairchild, I.J., Frisia, S., Spötl, C., Baker, A., Borsato, A., EIMF, 2010. High-resolution
786 sulphur isotope analysis of speleothem carbonate by secondary ionisation mass spectrometry.
787 Chemical Geology 271, 101-107.
788 Wynn, P.M., Fairchild, I.J., Borsato, A., Baker, A., Frisia, S., 2013. Biogeochemical cycling of sulphur
789 in the speleothem record. Biogeochemistry, 114, 255-267.
790 Wynn, P.M., Fairchild, I.J., Spötl, C., Hartland, A. Mattey, D., Fayard, B. & Cotte, M. 2014a.
791 Synchrotron X-ray distinction of seasonal hydrological and temperature patterns in speleothem
792 carbonate. Environmental Chemistry 11, 28-36.
793 Wynn, P., Loader, N., Fairchild, I., 2014b. Interrogating trees for isotopic archives of atmospheric
794 sulphur deposition and comparison to speleothem records. Environmental Pollution 187, 98-105.
795
796

Item	Period	References	Notes - Laboratory
ER dripwater	1993-1994	Borsato, 1995	Analyses made by *Agenzia Provinciale per la Protezione dell'Ambiente, Provincia Autonoma di Trento*. Bimonthly analyses from 06/1993 to 07/1994.
	1995-1997	Fairchild et al., 2000	In the paper only the mean dripwater SO_4 concentration for all the analyses was reported. Bimonthy analyses from 06/1995 to 12/1997.
	2002-2003 and 2013-2014	**this work**	*Istituto Agrario di San Michele all'Adige, Hydrochemistry laboratory*. Monthly analyses from 03/2002 to 05/2003.
	2004-2007	Wynn et al., 2013	Monthly analyses from 07/2004 to 12/2007.
ER soil water	2002-2003	**this work**	*Istituto Agrario di San Michele all'Adige, Hydrochemistry laboratory*. Bimonthly analyses from 08/2002 to 12/2003.
	2005-2007	Wynn et al., 2013	Monthly analyses from 10/2005 to 12/2007. The S concentration of 14 bedrock samples is also reported.
ER meteoric water	2005-2007	Wynn et al., 2013	Monthly analyses from 12/2005 to 12/2007.
Lavarone meteoric water	2004-2006	Wynn et al., 2013	Monthly analyses from 07/2004 to 11/2006.
Acquasanta spring water	1987-1989, 1991, 1999, 2002-2014	**this work**	*Servizio Geologico Provincia Autonoma di Trento*, and *Agenzia Provinciale per la Protezione dell'Ambiente*. Spot measurements. The data from 2008 – 2009 (monthly analyses) are also included in the internal report: Borsato, 2010.
ER78 stalagmite	1890 - 1998	Frisia et al., 2005; Wynn et al. 2013	Age model in Frisia et al., 2003; XRF intensity data in Frisia et al., 2005; single points SIMS data in Wynn et al., 2013.
	1890 - 1998	**this work**	Quantification of the XRF data.
	1994 - 2014	**this work**	Calculated theoretical S concentration on the basis of dripwater Sr/Ca and $D_{S.}$

Table 1. Synthesis of the sampling periods, sampling frequencies and data sources.

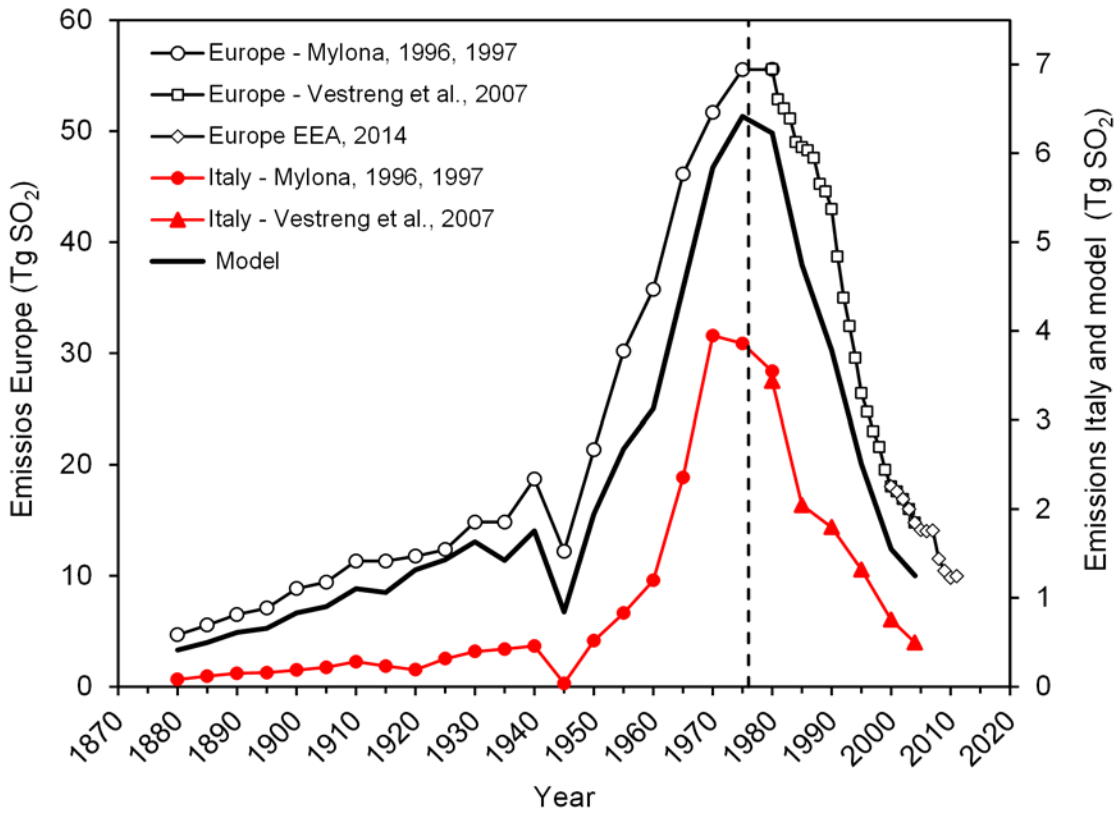

802

803 **Fig. 1**. Trend in sulphur dioxide emissions in Europe and Italy 1880-2011 AD. Sources: 1880-1975
804 from Mylona (1996, 1997); 1980-2004 from Vestreng et al. (2007); 2000-2011 from European
805 Environmental Agency (2014). The thick black line is the emission trend for the Southern Alps
806 modelled by accounting for Lagrangian moisture source diagnostic analysis (Sodemann and Zubler,
807 2010) (see cap. 6.1). The second part of the curves (1945 – 2011) shows an almost Gaussian normal
808 distribution centred on 1976 AD (dashed vertical line).

809

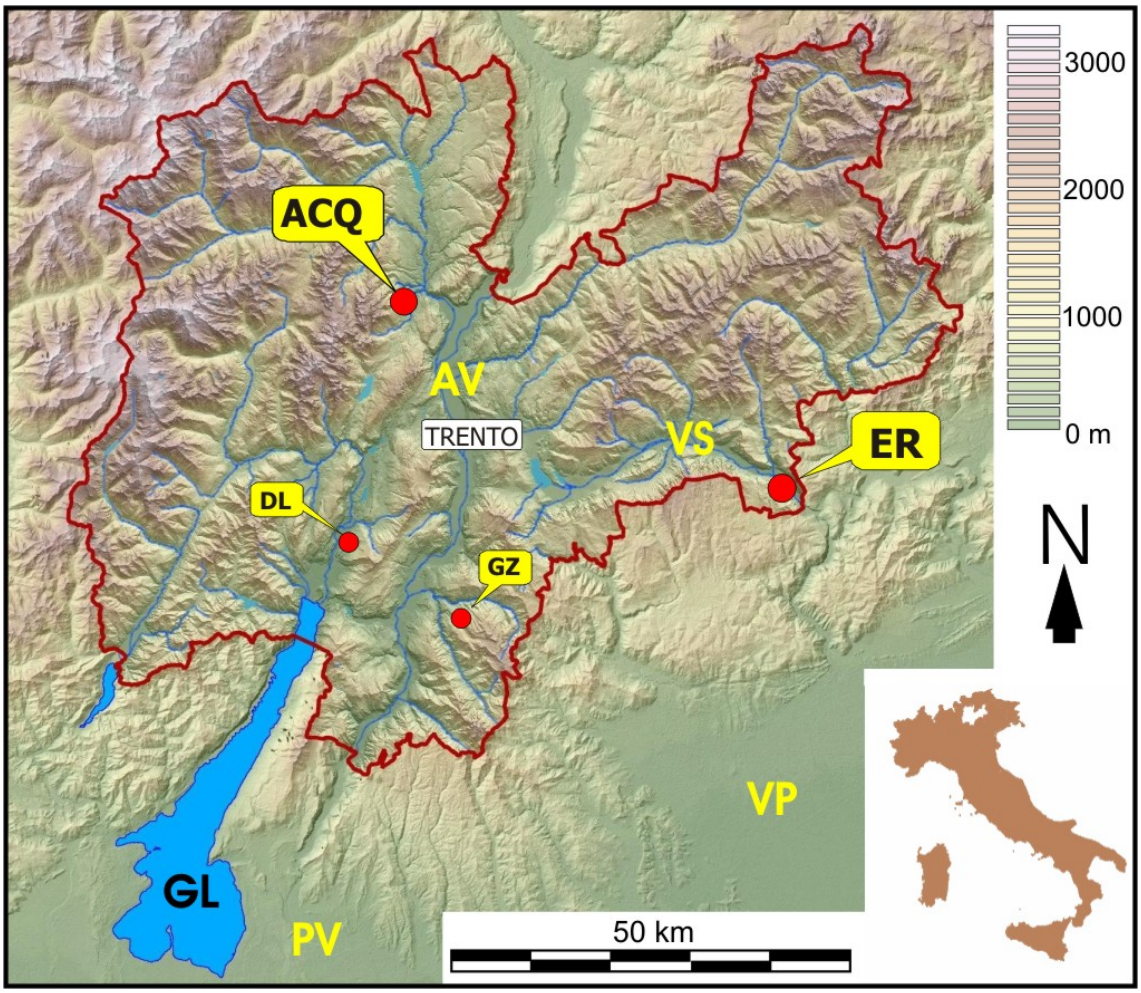

Fig. 2. Location of Grotta di Ernesto (ER) and Acquasanta karst spring (ACQ) on a digital elevation model of the Trento province. AV = Adige Valley; VS = Valsugana; PV = Po Valley; VP = Venetian Plain; GL = Garda Lake; DL = Bus del Diaol; GZ = Giazzera Cave.

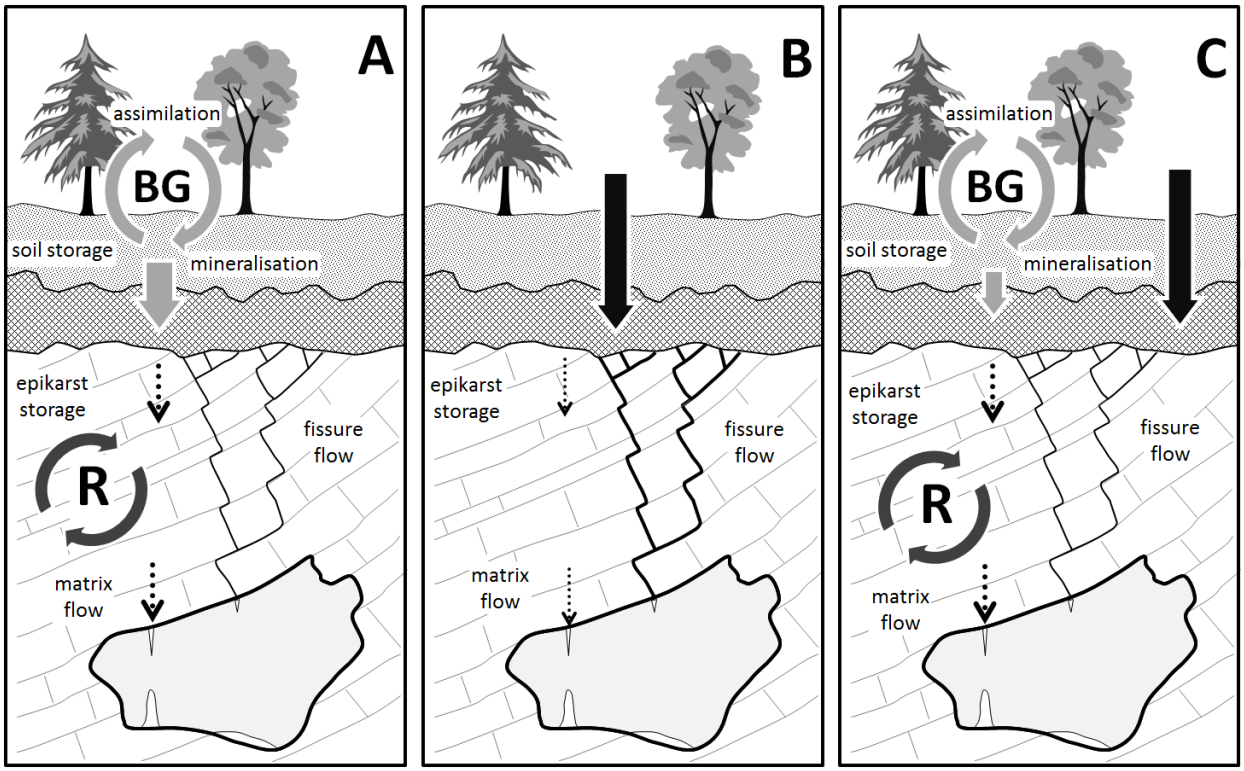

816

817 **Fig. 3**. Conceptual model for S cycling and transport in forested catchment karst inspired by the Grotta
818 di Ernesto system (modified after Wynn et al., 2013). Three different scenarios are illustrated: A) under
819 low sulphur atmospheric deposition S is biogeochemically (BG) modified by assimilation and stored in
820 the soil by mineralisation prior to entering the epikarst; B) during fast infiltration events S is
821 transmitted directly into the epikarst and to the cave via preferential fissure flow. C) during times of
822 high SO_2 atmospheric deposition the relative significance of biogeochemical cycling is diminished and
823 most of the S is transmitted unmodified to the epikarst. In the epikarst and in the aquifer S can be
824 transmitted into the cave via fissure flow or stored and subjected to redox cycling (R) in the matrix.
825 Each drip site in the cave is characterised by a unique combination of the above conditions and the
826 relative importance of each will vary through time as a response to changing environmental and
827 hydrological conditions.

828

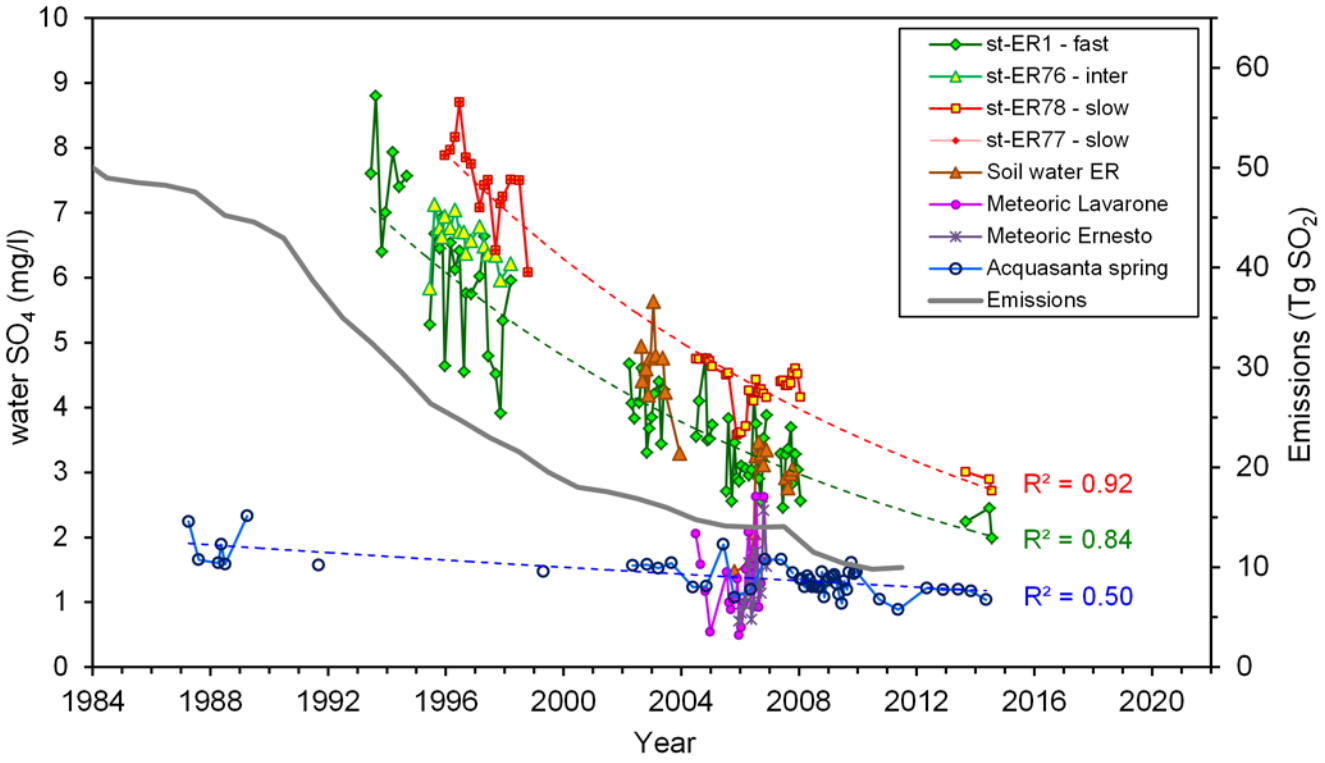

Fig. 4. Sulphate concentration time series for rainfall, soil water and cave dripwater at Grotta di Ernesto compared with the long trend in sulphate concentration in Acquasanta karst spring and sulphur dioxide emissions in Europe (cf. Fig. 1). For dripwater, green symbols and lines represent fast (st-ER1) and intermediate (st-ER76) flow, whereas red symbols and lines represent slow flow (st-ER77 and st-ER78). For data sources see Tab. 1.

836

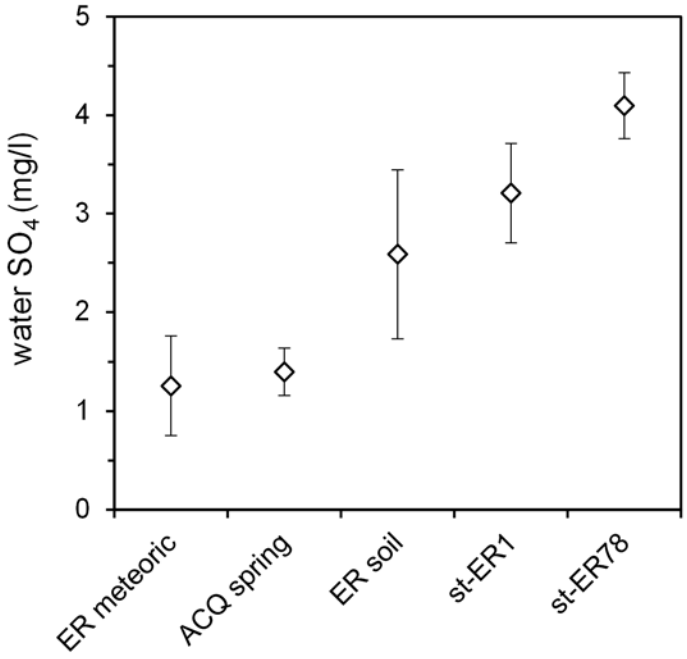

837

838 **Fig. 5.** Mean sulphate concentration and standard deviation in meteoric water, soil water and cave
839 dripwater at Grotta di Ernesto compared with the mean sulphate concentration of Acquasanta spring for
840 the period July 2005 – November 2006.

841

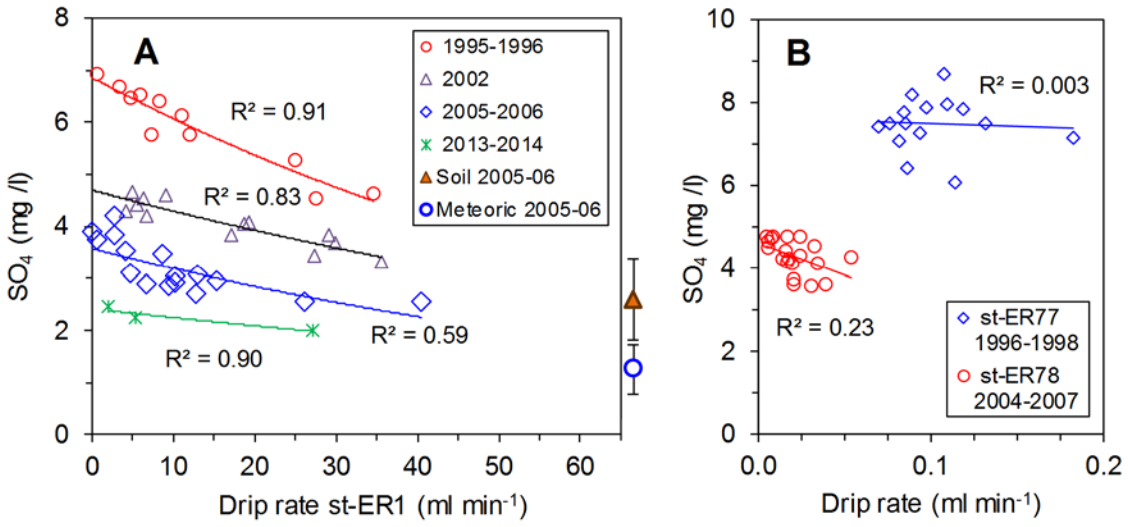

Fig. 6. Sulphate concentration vs. drip rate in stalactites st-ER1 (A), st-ER77 and st-ER78 (B) during selected time intervals. In (A) the mean sulphate concentrations in soil and meteoric water for 2005-2006 are also plotted outside the vertical secondary axis.

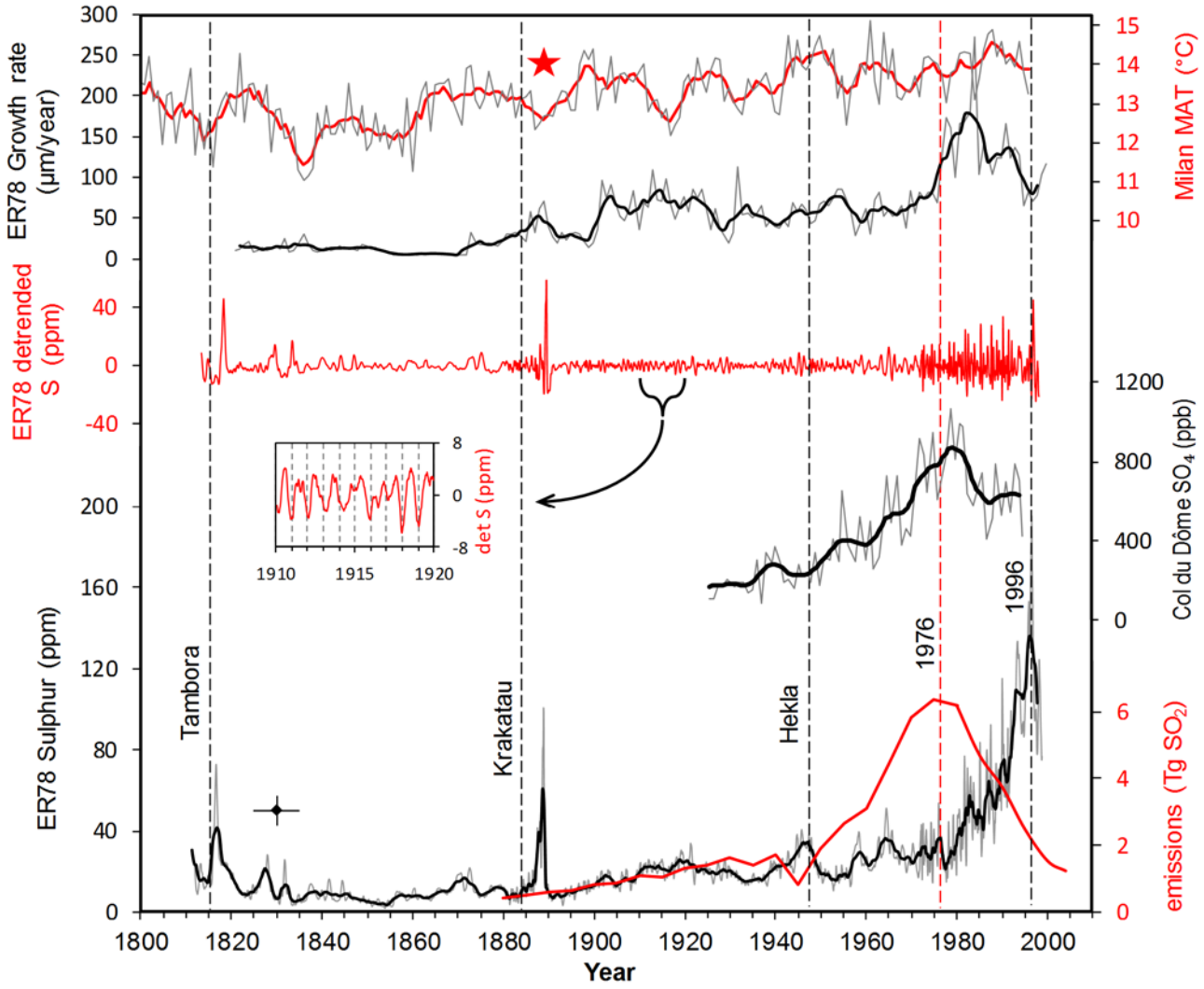

Fig. 7. Mean annual temperature in Milan (grey line: annual data; red line: 5 years running mean) (Maugeri and Nanni, 1998), ER78 lamina thickness (grey line: annual data; black line: 3 years running mean) (Frisia et al., 2003), S concentration (grey line: actual data; black line 2 years Gaussian filter) and detrended S concentration in ER78 stalagmite (data from Frisia et al., 2005, 2008) compared with the modelled sulphur dioxide emissions for the Southern Alps (cf. Fig. 1) and the Col du Dôme ice core summer sulphate record (grey line: actual data; black line: first component of single spectra analysis with a 5 year time window) (Preunker et al., 2001). The dashed vertical lines mark: Tambora (April 1815), Krakatau (August 1883) and Hekla (March 1947) eruptions, the peak of the S emissions (1976) and the maximum value of the ER78 S peak (1996). The structure of the detrended S concentration identifies two distinctive short-lived peaks attributed to the Tambora and Krakatau eruptions as well as a clear annual structure between 1890 and 1970, also highlighted in the blow-up panel. The red star

marks the end of the Little Ice Age in the Italian Alps. The cross on the bottom left corner visualises the mean error (±5 years) in the oldest part of the record (1810 – 1890) based on the original lamina counting (Frisia et al., 2003), whereas for the recent part of the record (1970 – 1996) the estimated error is ±1 year.

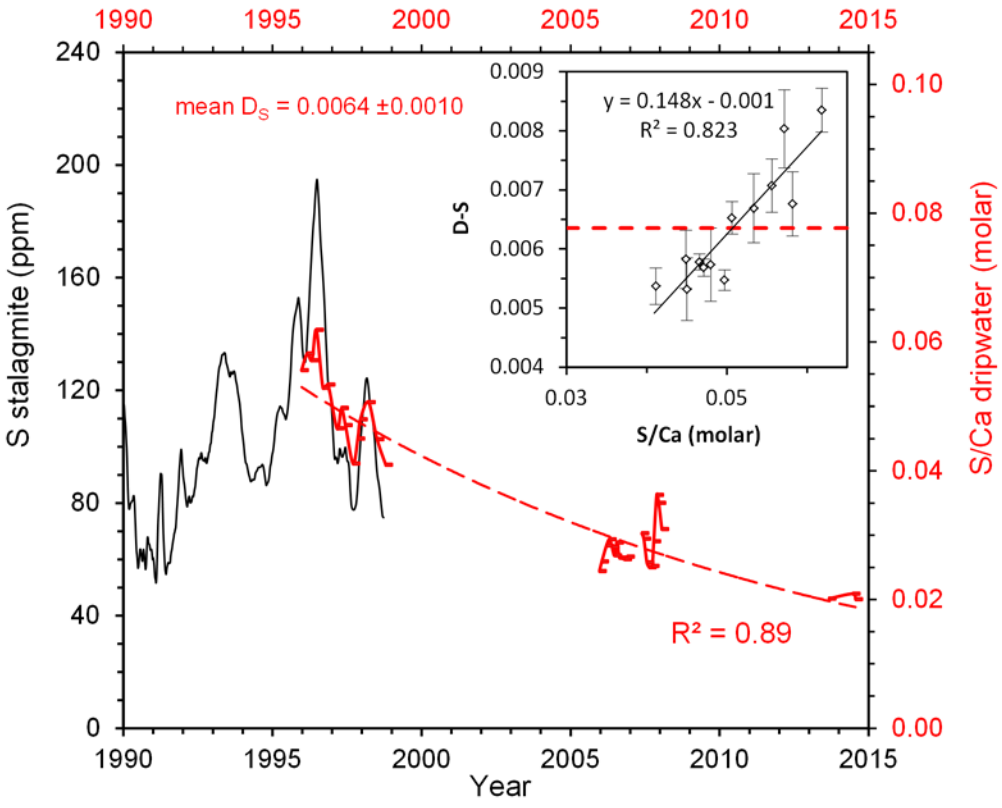

865

866 **Fig. 8.** Measured S concentration in stalagmite ER78 (original data from Frisia et al., 2005, 2008)
867 compared with the dripwater S/Ca ratio (red dots and line). The dashed red line is the exponential
868 regression of the dripwater S/Ca data (R^2=0.89, p < 0.0001). Inset: correlation between sulphur
869 partition coefficient (D_S) and dripwater S/Ca calculated in the overlapping period (1995-1998). The
870 age uncertainty based on lamina counting in this part of the stalagmite is ±1 year (Frisia et al., 2003).

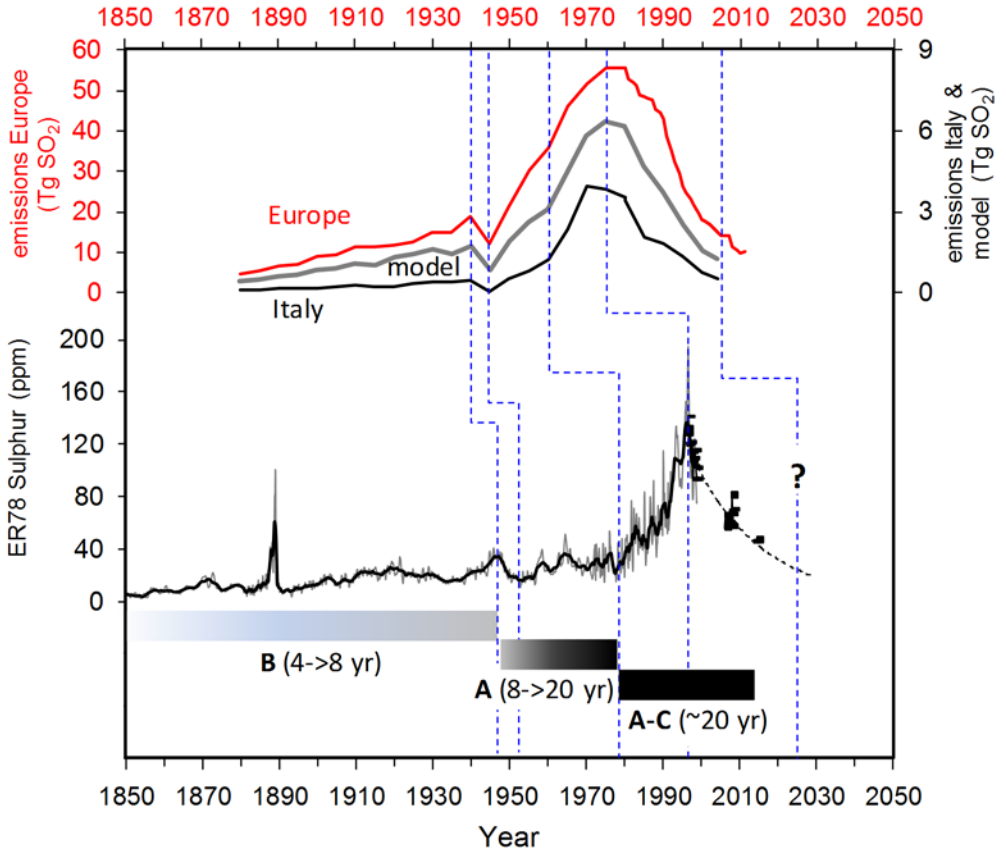

Fig. 9. Sulphur time-series for ER78 stalagmite (grey line actual data, black line 2 years Gaussian filter, Frisia et al. 2005, 2008) compared with the sulphur dioxide emissions (cf. Fig. 1). For ER78 stalagmite the theoretical series reconstructed by the measured dripwater S/Ca ratio (black dots and line, cf. Fig. 8) and the projected trend until 2030 (dashed black line) are also shown. The blue dashed lines identify suggested correlation between the series, while the grey bars at the bottom indicate the reconstructed hydrological scenario (A to C in Fig. 3) and the corresponding mean delay in the stalagmite S series.

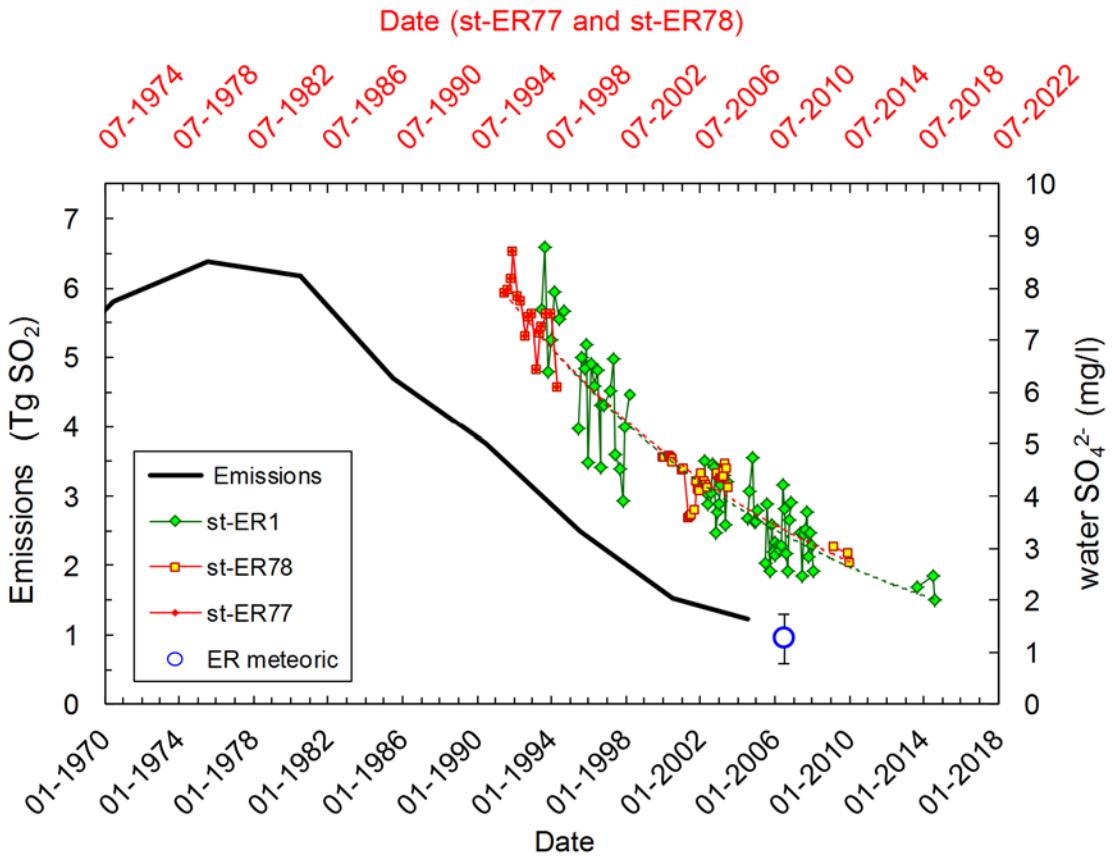

Fig. A1. Comparison of sulphur time-series. The series st-ER77 and st-ER78 have been offset by 4.5 years in order to best match series st-ER1. The offset represents the additional delay related to S retention in the aquifer matrix with respect to the fast fissure flow. The modelled S emissions (cf. Fig. 1) and the mean sulphate concentrations in meteoric water for 2005-2006 are also plotted.

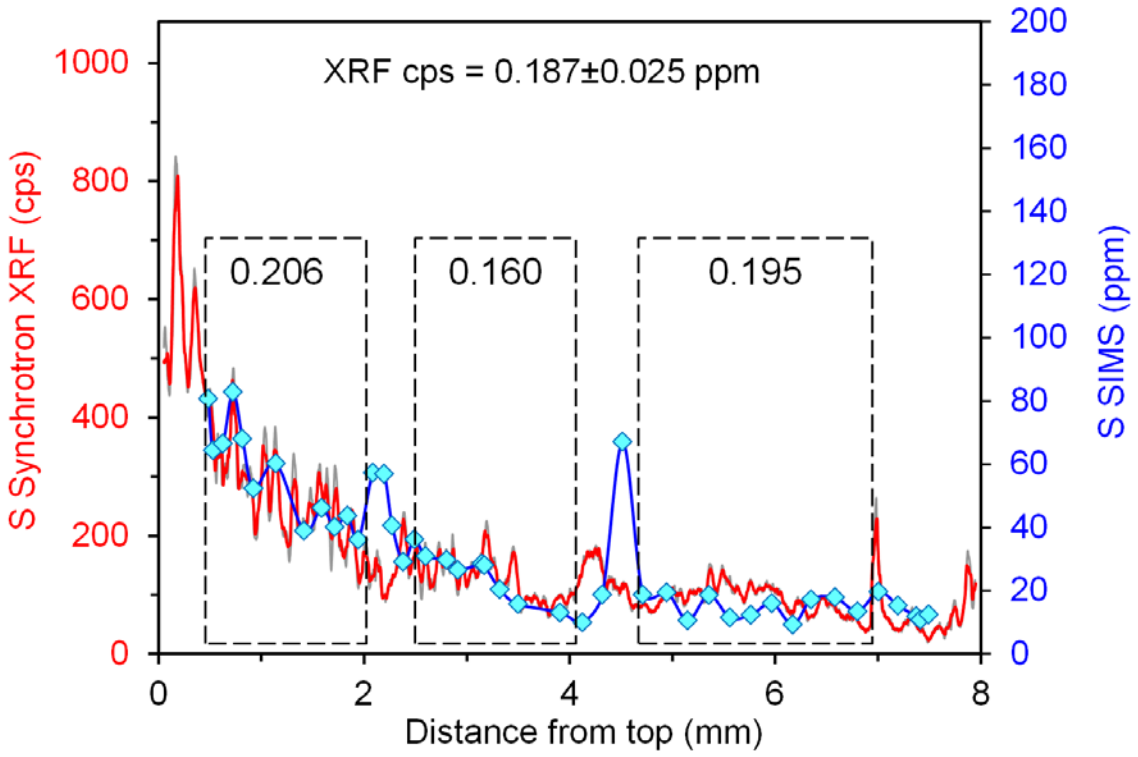

887

888 **Fig. A2.** Calibration of sulphur SR-XRF data (Frisia et al., 2005) on the basis of SIMS analyses (Wynn
889 et al., 2008) for ER78 stalagmite. Measurements were carried out on two physically different slabs and,
890 consequently, we choose three separate parts of the scans in order to avoid the presence of distinctive
891 peaks in the two scans possibly related to grain inclusions. The linear calibration value (XRF cps =
892 0.187 ±0.025 ppm) was calculated as the arithmetic mean between values obtained in the three regions
893 highlighted by dashed boxes.